HHS Public Access

Author manuscript

Dev Cell. Author manuscript; available in PMC 2024 April 08.

Published in final edited form as:

Dev Cell. 2023 December 18; 58(24): 2867–2880.e7. doi:10.1016/j.devcel.2023.10.012.

Transcription factor NFYa controls cardiomyocyte metabolism and proliferation during mouse fetal heart development

Miao Cui[1,2,*], **Svetlana Bezprozvannaya**[3], **Tian Hao**[1], **Abdallah Elnwasany**[4], **Luke I. Szweda**[4], **Ning Liu**[3], **Rhonda Bassel-Duby**[3], **Eric N. Olson**[3,5,*]

[1]Department of Cardiology, Boston Children's Hospital, 300 Longwood Ave, Boston, MA 02115, USA

[2]Department of Genetics, Harvard Medical School, 77 Avenue Louis Pasteur, Boston, MA 02115, USA

[3]Department of Molecular Biology, Hamon Center for Regenerative Science and Medicine and Sen. Paul D. Wellstone Muscular Dystrophy Specialized Research Center, University of Texas Southwestern Medical Center, 5323 Harry Hines Boulevard, Dallas, TX 75390, USA

[4]Division of Cardiology, Department of Internal Medicine, University of Texas Southwestern Medical Center, 5323 Harry Hines Boulevard, Dallas, TX 75390, USA

[5]Lead contact

SUMMARY

Cardiomyocytes are highly metabolic cells responsible for generating the contractile force in the heart. During fetal development and regeneration, these cells actively divide but lose their proliferative activity in adulthood. The mechanisms that coordinate their metabolism and proliferation are not fully understood. Here, we study the role of the transcription factor *NFYa* in developing mouse hearts. Loss of *NFYa* alters cardiomyocyte composition, causing a decrease in immature regenerative cells and an increase in trabecular and mature cardiomyocytes, as identified by spatial and single-cell transcriptome analyses. *NFYa*-deleted cardiomyocytes exhibited reduced proliferation and impaired mitochondrial metabolism, leading to cardiac growth defects and embryonic death. NFYa, interacting with cofactor SP2, activates genes linking metabolism and proliferation at the transcription level. Our study identifies a nodal role of NFYa in regulating prenatal cardiac growth and a previously unrecognized transcriptional control mechanism of heart metabolism, highlighting the importance of mitochondrial metabolism during heart development and regeneration.

Graphical Abstract

*Correspondence: miao_cui@hms.harvard.edu (M.C.), eric.olson@utsouthwestern.edu (E.N.O.).

AUTHOR CONTRIBUTIONS

M.C., S.B., T.H., A.E., and L.I.S. designed and performed experiments. M.C., S.B., and L.I.S. performed the data analysis. N.L. and R.B.-D. contributed to the discussion. M.C., N.L., and E.N.O. wrote the manuscript.

DECLARATION OF INTERESTS

The authors declare no competing interests.

SUPPLEMENTAL INFORMATION

Supplemental information can be found online at https://doi.org/10.1016/j.devcel.2023.10.012.

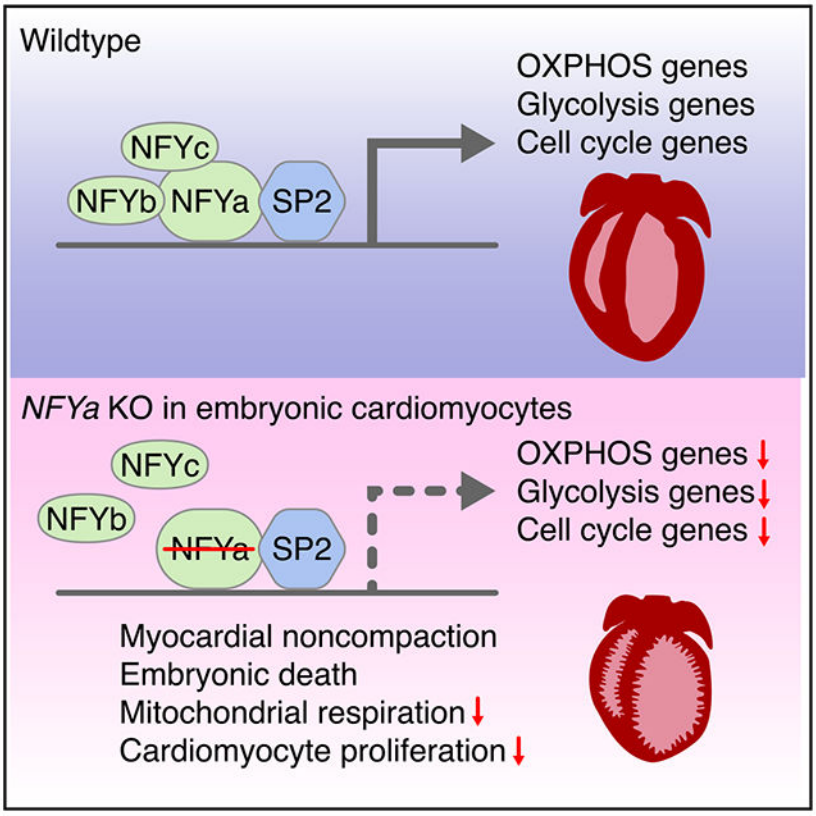

In brief

In this study, Cui et al. identified a critical role of the nuclear transcription factor Y in regulating mitochondrial metabolism and proliferation in heart muscle cells of the developing mouse heart.

INTRODUCTION

Cardiomyocytes (CMs) are specialized heart cells with contractile functions. During embryogenesis, CMs proliferate extensively, but their proliferation potential diminishes rapidly post-birth in mice.[1] Concomitant with the reduction in proliferation, CMs undergo maturation to support the high contractile demands of the adult heart.[2] Disrupting this transition, through premature cell-cycle exit or maturation, can cause cardiac developmental defects,[3,4] which represent the most common human birth defect. Concurrent with CM maturation is the heart's diminishing regenerative ability post-injury.[5,6] Although adult mammalian hearts lack regeneration ability, hearts from neonates can regenerate after injuries,[5,7,8] but this potential is lost by postnatal day (P) 7 in mice. This transient regenerative capacity is also present in large mammals, such as pigs[9,10] and possibly humans.[11] Reawakening the dormant cardiac regenerative capacity in adults offers potential heart repair therapies.

During neonatal heart regeneration, new CMs arise exclusively from preexisting CMs through proliferation.[8] Whether this regenerative capacity is specific to a subset of CMs with unique regenerative abilities remains unclear. Using single-nucleus RNA sequencing

(snRNA-seq), we previously identified a distinct CM subpopulation, CM4, in newborn mice that exhibits regenerative features post-injury governed by the transcription factor NFYa.[7] NFYa is the DNA-binding subunit of the nuclear transcription factor Y (NF-Y), which regulates the expression of many cell-cycle, housekeeping, and cell-type-specific genes.[12-17] Although NFYa is known to regulate skeletal muscle differentiation[18-20] and proliferation of cardiac fibroblasts,[21] its role in CMs during development and disease remains largely unknown. Our previous study showed that *NFYa* expression is enriched in CM4 cells and that overexpression of NFYa promotes CM proliferation,[7] suggesting a role in regulating heart growth. Indeed, zebrafish with global *nfya* knockdown developed severe cardiac growth defects.[22]

Here, we investigated the role of NFYa in mammalian heart development using CM-specific knockout mice. Mice lacking *NFYa* in CMs died pre-birth with underdeveloped hearts, exhibiting noncompaction and hypoplastic phenotypes. By integrating data from snRNA-seq, single-nucleus transposase-accessible chromatin sequencing (snATAC-seq), and spatial transcriptomics, we show that *NFYa* deletion changes CM composition in the fetal heart by decreasing the number of immature CMs that are transcriptionally similar to neonatal CM4 cells and increasing trabecular and mature CMs. We identified metabolic and proliferative defects in *NFYa*-deleted hearts and showed that NFYa functions with its cofactor SP2 to directly control expression of metabolic genes. Our findings demonstrate a nodal role of NFYa in regulating metabolism and proliferation during heart development and highlight its importance in fetal heart growth and the establishment of neonatal regenerative CMs.

RESULT

Cardiomyocyte-specific deletion of *NFYa* causes embryonic lethality, cardiac hypoplasia, and noncompaction

NFYa mRNA is expressed in mouse embryonic hearts, but its expression decreases after embryonic (E) day 12 and further declines after birth (Figure S1A). At postnatal (P) day 1, *NFYa* expression is detected in both atria and ventricles at similar levels (Figure S1B) but is significantly reduced in adult ventricles (Figure S1D). Although ubiquitously expressed in diverse cardiac cells (Figure S1D), CM expression of *NFYa* decreases from P1 to P14 both at RNA and protein levels (Figures 1A and S1E).

To study the function of NFYa in embryonic and perinatal CMs when it is highly expressed, we created CM-specific *NFYa* deletion mice (*NFYa* cKO) by crossing *NFYa*$^{fl/fl}$ mice[17] with αMHC-Cre transgenic mice. Cre expression starts around E10,[23] ensuring efficient embryonic and postnatal deletion of *NFYa* (Figure S1F). *NFYa* cKO mice with the *αMHC-Cre;NFYa*$^{fl/fl}$ genotype were observed in less than 5% of progeny at P1, as opposed to 25% based on Mendelian ratios, suggesting embryonic lethality (Figure 1B). The few that survived at P1 developed cardiac dilation and interstitial fibrosis and died by P20 (Figures S1G-S1I). These results showed that *NFYa* deletion in CMs causes lethality with complete penetrance. Given that most *NFYa* cKO mice die before birth, we focused on embryonic heart development.

At E15.5, *NFYa* cKO embryos were detected at Mendelian ratios (Figures 1B and S1J). Although smaller, E15.5 *NFYa cKO* hearts had no apparent anatomical defects with proper specification of cardiac chambers and valves analyzed by wholemount imaging (Figures 1C, S1K, and S1L). However, they developed a distinct cardiac noncompaction phenotype with decreased thickness of ventricular compact zone and interventricular septum and increased trabecular thickness (Figures 1D-1F).

Abnormalities in CM proliferation are associated with noncompaction cardiomyopathy.[3,24,25] We analyzed CM proliferation by immunofluorescence staining of phospho-histone H3 (pH3), a marker of mitosis.[26] *NFYa* cKO hearts showed a subtle (3.8% versus 4.5%, n = 5 for cKO, n = 3 for control), but statistically significant decrease in the percentage of pH3-positive CMs compared with control hearts (α*MHC-Cre;NFYa*$^{fl/+}$) (Figures 1G and 1H), suggesting a G2-M phase transition defect. *NFYa* cKO hearts also showed a decrease in the percentage of Aurkb-positive midbodies, suggesting a cytokinesis defect (Figures 1I and 1J). Thus, loss of *NFYa* in CMs causes lethality with full penetrance and results in cardiac noncompaction with hyper trabeculation and decreased CM proliferation.

Multi-modal single-cell analysis identifies distinct cardiomyocyte populations in embryonic hearts

To study the mechanisms underlying the embryonic lethality of *NFYa* cKO mice, we performed joint snRNA- and snATAC-seq on PCM1^{+} CM nuclei from *NFYa* cKO and wild-type (WT) hearts at E16 using the Multiome from 10x Genomics (Figure 2A). We performed a “weighted-nearest neighbor” (WNN) analysis to integrate both RNA sequencing (RNA-seq) and ATAC-seq data within the same cell to achieve a joint definition of cellular state.[27] Analysis of 7,878 sequenced CM nuclei from WT and *NFYa* cKO hearts identified 13 clusters with distinct gene expression signatures (Figures 2B, 2C, and S2A; Table S1).

To identify CMs based on their anatomic locations, we performed spatial transcriptome analysis on sections collected from *NFYa* cKO and WT hearts at E15.5. Using the Visium from 10× Genomics, we captured 373 and 333 spatial spots for *NFYa* cKO and WT hearts, respectively (Figure S2B). Each spot captured multiple cells; thus, we deconvoluted the underlying composition of cell types by integrating the spatial transcriptome data with Multiome datasets. This analysis calculated the fraction of each CM cluster per spatial spot, revealing their anatomic distribution (Figures 2D and S2C). Furthermore, by integrating snRNA and snATAC data, we identified key transcriptional regulators of each cluster based on RNA expression and chromatin accessibility (Figure 2E).

Ventricular CMs—Seven CM populations were identified in embryonic heart ventricles. Three, expressing markers *Tnni1, Myh7*, and *Acta2*, were categorized as fetal ventricular CMs,[28-30] labeled F-VCM1 to F-VCM3 (Figure 2C). Spatial analysis revealed F-VCM1 cells throughout the ventricles, F-VCM2 preferentially near ventricular trabeculae, and F-VCM3 in the ventricular compact zone and interventricular septum (Figures 2D and S2C). *Esrra, Nkx2-5, Usf2, Hey2*, and *Hes6* were identified as top transcription factors enriched in

F-VCM1 cells at both expression and motif accessibility levels (Figure 2E). These factors were not enriched in F-VCM2 and F-VCM3 cells, which instead shared a common set of regulators including *Erg, Elk3, Ets1*, and *Fli1* (Figure 2E).

We identified two CM populations, T-VCM1 and T-VCM2, enriched in the trabecular region, especially in *NFYa* cKO hearts with hyper-trabeculation (Figures 2D and S2C). These cells expressed known trabecular genes like *Slit2, Mest*, and *Sema3a* (Figure 2C)[31-33] and new trabecular markers, *Mpped2*, and *Rbfox1* (Figure S2A).

Three CM populations, M-VCM1 to M-VCM3, expressed maturation genes like *Ryr6* and *Dmd* and were dispersed throughout the ventricles or enriched in the compact myocardium and interventricular septum (Figures 2C, 2D, and S2C). These cells expressed higher levels of *Tnni3K* (Figure S3A), a factor that regulates CM binucleation,[34,35] and the DNA damage sensor *Brca1* (Figure S3B). DNA damage causes CM cell-cycle arrest and binucleation, which are hallmarks of mature CMs.[36,37] These cells shared upstream regulators *Esrra* and *Hey2* with F-VCM1 but also expressed *Mef2, Meis1*, and *Meis2*, which promote CM cell-cycle arrest (Figure 2E).[38]

CME+—We identified a CM population expressing extracellular matrix (ECM) genes like *Col1a1* and *Col1a2* (Figures 2C and S2A). These CMs, termed CME+, were previously identified in embryonic mouse hearts.[39] ECM genes, usually expressed by fibroblasts, were further analyzed in our scATAC-seq data to exclude potential RNA contamination. Clear ATAC peaks were observed at loci of both CM marker *Myh7* and fibroblast marker *Col1a2*, indicating a combined CM/fibroblast gene signature (Figures S3C and S3D). These CME+ cells were mostly near the epicardium (Figures 2D and S2C) and regulated by factors *Maf, Cebpb, Sp3*, and *Klf4* (Figure 2E).

Atrioventricular canal CMs (AVC-CM)—We identified a population of CMs mapped to the atrioventricular canal of the heart (Figures 2D and S2C), expressing *Gpc6* (Figure 2C), a gene that has been implicated in cell growth control.[40] Gene ontology analysis of atrioventricular canal CMs (AVC-CMs) marker genes were enriched for pathways that regulate ECM organization and aortic valve morphogenesis (Figures S3E and S3F), suggesting active remodeling at E15.

Atrial CMs—We identified two atrial CM groups, ACM1 and ACM2, expressing known atrial markers *Fgf12* and *Myl7* (Figure 2C).[41] Differential gene expression analysis showed that ACM1 cells expressed higher levels of genes that regulate mitochondrial metabolism and ribosome biogenesis, whereas ACM2 cells exhibited a muscle contractile gene signature (Figures S3G-S3I). *Tbx5* and *Tbx20* were identified as key regulators of both atrial populations (Figure 2E).[42-45] *Nkx2-5* and *Hes6* were identified as ACM1-specific regulators, whereas *Mga* was exclusively expressed in ACM2 (Figure 2E).

Cardiac conduction system—We identified a CM cluster that expresses cardiac conduction system (CCS) markers, such as *Rgs6, Cacna1d*, and Ntm[46] (Figures 2C and S2A), predominantly located in the crux region of the heart (Figures 2D and S2C), suggesting that they form the atrioventricular node (AVN) and His bundle (His).

Transcription factor analysis identified known regulators of the CCS, such as *Tbx5, Tbx20*, and *Pitx2*,[45,47,48] as well as *Mef2a, Mef2b*, and *Lef1* whose functions in the CCS are less understood (Figure 2E).

NFYa deletion alters cardiomyocyte composition in the embryonic heart

Having identified the different CM populations in embryonic hearts, we next compared their abundance between WT and *NFYa* cKO hearts. *NFYa* deletion decreased atrial ACM1 cells from 2.3% in WT to 0.5% in cKO hearts and F-VCM1 cells from 16.7% in WT to 10% in cKO hearts (Figure 2F). This reduction of atrial CMs is consistent with the smaller atrial size in *NFYa* cKO hearts (Figures 2D and S1K). *NFYa* deletion also slightly increased the fraction of M-CM1 cells and AVC-CM cells (Figure 2F). Consistent with the hyper-trabeculation phenotype, trabecular CM populations (T-VCM1 and T-VCM2) were increased in *NFYa* cKO hearts (from 3.7% and 5.8% in WT to 6.3% and 8.4% in cKO hearts, respectively).

After initially identifying NFYa in postnatal regenerative CM4 cells in our previous study,[7] we next explored the impact of *NFYa* deletion on CM4 cells. To identify embryonic CMs that are orthogonal to CM4 cells, we analyzed the expression of CM4 markers (Figure 2G) and curated a CM4 cell score for each embryonic CM (see STAR Methods). Our analysis showed that the three fetal populations (F-VCM1-3), A-CM1, and CME+ cells have the highest CM4 cell scores (Figure 2H) and express higher levels of immature CM markers *Tnni1, Myh7*, and *Acta2* (Figure 2C), consistent with our previous observation that CM4 cells are immature.[7] Importantly, the fraction of embryonic CM4 cells dropped from 43.9% in WT to 32.8% in *NFYa* cKO hearts (Figure 2I), underscoring *NFYa*'s role in regulating CM4 cells. To assess if reduced CM4 cells in *NFYa* cKO hearts were due to proliferation defects, we examined G2/M phase CMs with our snRNA-seq data. Both WT and *NFYa* cKO CM4 cells showed higher G2/M proportions than other CMs (Figure S3J), suggesting their proliferative capability. Yet, *NFYa* deletion notably diminished G2/M proportions in CM4 cells (Figure S3J), implying that *NFYa* deletion mainly impacted immature CMs resembling neonatal regenerative CM4 cells.

NFYa deletion causes metabolic defects in embryonic hearts

We next investigated the molecular changes in *NFYa*-deleted CMs. Differential gene expression analysis on combined CM clusters from our snRNA-seq data revealed ectopic upregulation of cardiac stress genes (*Nppa* and *Nppb*) and precocious activation of maturation genes (*Cacna1d* and *Pdlim 3/5*) upon *NFYa* deletion (Figure 3A). Genes significantly downregulated included fetal CM genes, such as *Tnni1, Myh7*, and *Acta2* (Figure 3A; Table S2), suggesting loss of an immature gene signature in *NFYa*-deleted CMs. Gene ontology analysis identified downregulated pathways regulating mitochondrial metabolism, such as cellular respiration, oxidative phosphorylation (OXPHOS), and NADH dehydrogenase complex assembly (Figure 3B). Although embryonic hearts primarily use anaerobic glycolysis for energy production, mitochondrial respiration is also critical for cardiac development.[49-51] We found that genes encoding mitochondrial complexes and mitochondrial ATP synthases were significantly downregulated upon *NFYa* deletion (Figures S4A and S4B).

To study the extent to which embryonic hearts rely on NFYa for mitochondrial respiration, we analyzed rotenone-sensitive NADH oxidation as a direct measurement of mitochondrial electron transport chain activity.[52] Using tissue lysates collected from E15 hearts, we observed a significant reduction of NADH oxidation in *NFYa* cKO hearts (Figure 3C), suggesting mitochondrial dysfunction. Mitochondrial DNA copy number was not changed (Figure S4C). Analysis of oxygen consumption rates (OCRs) showed that basal respiration, maximal respiration, and ATP production were all significantly reduced in $NFYa^{fl/fl}$ CMs infected with Cre adenovirus (Ad-Cre) compared with those infected with Ad-LacZ (Figures 3D-3G), demonstrating compromised mitochondrial respiration in *NFYa*-deleted CMs. Additionally, *NFYa* deletion led to reduced expression of genes crucial for glycolytic metabolism (Figure S4D).

Through targeted metabolomics analysis on E15 control and *NFYa* cKO hearts, we found 53 significantly downregulated metabolites in *NFYa* cKO hearts (Figures S4E and S4F), associated with several catabolic and anabolic metabolic processes (Figure 3H). The top enriched metabolic pathway was citrate acid cycle (TCA) (Figure 3I), as TCA intermediates, succinyl-CoA, succinate, and alpha-Ketoglutarate (AKG) were all significantly reduced (Figure S4F). Corroborating changes in metabolites, genes encoding key metabolic enzymes regulating TCA cycle, such as *Idh2, Sdhb, Fh1*, and *Mdh1/2*, were downregulated in *NFYa*-deleted CMs (Figure S4G). Key glycolysis intermediates, fructose 6-phosphate and fructose 1,6-biphosphate, were also reduced in *NFYa* cKO hearts (Figures 3J and S4F), aligning with the reduced glycolytic gene expression (Figure S4D), indicating a defect in glycolysis.

Downregulated metabolites in *NFYa* cKO hearts also enriched for glutathione metabolism, purine metabolism, and amino sugar and nucleotide sugar metabolism pathways (Figure 3H). Glutathione metabolism plays an important role in the antioxidant defense,[53] the reduced levels of glutathione disulfide, NADPH, and $NADP^+$ in *NFYa* cKO hearts indicate a redox imbalance (Figure S4H). Indeed, we observed increased reactive oxygen species (ROS) in $NFYa^{fl/fl}$ CMs infected with Ad-Cre compared with Ad-Lac-infected cells (Figures 3K and S7K). Reduction in purine metabolism indicates decreased availability of nucleotides for DNA and RNA synthesis, which has been shown to impair cell growth and division.[54] Fatty acid (carnitine and 3-hydroxycarnitine) and phospholipid derivatives (PE, PC, and PS) were increased in *NFYa* cKO hearts (Figures S4F and S4L), suggesting a shift to lipid metabolism. Lipid metabolism is linked to cell-cycle arrest and maturation of CMs,[55] likely also contributing to the reduced proliferation and precocious maturation of *NFYa*-deleted CMs. Together, our results showed that *NFYa* cKO hearts display significant changes of several metabolic processes, including redox imbalance, aberrant mitochondrial metabolism, and glycolysis, which collectively disrupt CM development and proliferation.

NFYa regulates metabolic genes

To study whether NFYa directly regulates the expression of metabolic genes, we performed chromatin immunoprecipitation followed by sequencing (ChIP-seq) in neonatal rat ventricular CMs (NRVMs) that overexpressed TY1-tagged NFYa. NFYa has been shown to function as both an activator and a repressor[56]; therefore, we also performed ChIP-seq for the active histone mark H3K27ac. We identified 3,984 chromatin regions that were bound

by NFYa (Figures 4A and S5A; Table S3). Motif analysis of these regions identified the NFYa DNA-binding site as the top enriched motif (Figure 4B). Most NFYa-bound regions were also marked by H3K27ac (Figure 4A), indicating that NFYa primarily functions as an activator in CMs. NFYa-bound regions were associated with genes regulating mitotic cell-cycle process and chromosome organization (Figure 4C), corroborating the known roles of NFYa in proliferation and as a pioneer factor,[57,58] and also genes regulating the TCA cycle and respiratory electron transport activity (Figure 4C).

We next intersected the differentially expressed genes by *NFYa* deletion (Figure 3A) with those that were bound by NFYa. This analysis allowed us to delineate direct transcriptional effects versus secondary effects in CMs upon *NFYa* deletion. We found that many cell-cycle genes and metabolic genes, including genes regulating glycolysis (*Adha, Tpi1, Aldoa*, and *Pgk1*) and OXPHOS (*Atp5b, Atp5a1*, and *Cox8a*), were direct targets of NFYa, as evidenced by NFYa binding at gene promoters (Figures S5B and S5C) and their transcriptional downregulation in *NFYa*-deleted CMs (Figures S4A, S4B, and S4D). Cardiac fetal genes *Tnni1, Myh7*, and *Acta2*, although downregulated by *NFYa* deletion, showed no detectable NFYa binding (Figures S5B and S5D), indicating indirect regulation by NFYa. NFYa binding was widespread at promoter regions of actively transcribed genes (marked by H3K27ac) regulating OXPHOS and glycolysis (Figures 4D and 4E), further supporting NFYa as a critical transcription activator of cardiac metabolism. Consistent with its role in controlling proliferation, NFYa binding was detected at active cell-cycle genes (Figure 4F).

To determine if NFYa binding is essential for transcription of metabolic genes, we removed its binding sites from the promoters of *Pgk1, Atp5b*, and *Cox8a* (Figure 4G). Using GFP reporter expression, we found that the WT promoters drove robust expression compared with a minimal promoter (Figure 4H). The reporter activity diminished significantly when NFYa binding sites were removed (Figure 4H), showing a functional requirement of NFYa binding for the transcriptional activity of these promoters.

NFYa associates with SP2

NFYa is known to bind cofactors to elicit context-dependent regulatory functions.[59,60] To identify cardiac cofactors of NFYa, we analyzed factors with co-enriched DNA-binding motifs at NFYa-bound regions, which identified KLF1/3/5, SP1/2/5, and En1 (Figure 4B). Using a proximity labeling assay in NRVMs expressing an NFYa and miniTurbo fusion protein,[61] we identified 201 potential NFYa-interacting proteins (Figures S5E and S5F), including YAP1, a known CM proliferation regulator.[62,63] Of the factors whose DNA-binding motifs were co-enriched with NFYa, SP2 was also identified to interact with NFYa by proximity labeling assay.

In HEK293 cells co-expressing $NFYa^{FLAG}$ with either $SP2^{Myc}$or $LacZ^{Myc}$, $SP2^{Myc}$, not $LacZ^{Myc}$, was detected when pulling down NFYa with an anti-FLAG antibody, confirming the direct interaction between NFYa and SP2 (Figure 4I). This direct binding was validated at the endogenous protein level in CMs isolated from P2 mouse hearts (Figure S5G). Moreover, SP2 binding sites were identified adjacent to the NFYa sites at the promoter regions of *Pgk1, Atp5b*, and *Cox8a*. Deleting SP2 sites significantly reduced the promoter-

driven reporter expression (Figure 4H), suggesting that NFYa and SP2 binding is essential for the expression of these metabolic genes.

DISCUSSION

We identified NFYa as being essential for coupling cell-cycle and metabolic gene transcription in fetal CMs. NFYa expression is required for normal heart development and its CM-specific deletion leads to embryonic lethality. NFYa plays a pivotal role in regulating the metabolic state of the embryonic heart, highlighting its potential as a therapeutic target for modulating metabolism in cardiovascular disease.

A context-dependent role of NFYa in regulating metabolism

The NF-Y complex, although extensively studied for cell proliferation,[57] is less understood for its metabolic function. Our findings demonstrate that NFYa interacts with SP2 in fetal CMs, leading to the transcriptional activation of genes that regulate glycolytic and oxidative metabolism. The metabolic function of NF-Y is context-dependent. In HepG2 cells during sterol depletion, NF-Y collaborates with SREBP1 to upregulate genes involved in cholesterol and fatty acid metabolism.[13,14,64] In cancer cells, NF-Y activates glycolytic genes and *de novo* lipid biosynthetic pathways but is neutral or repressive toward mitochondrial respiratory genes.[65] NFYa promotes mitochondrial metabolism in prostate cancer, although direct transcriptional regulation was not examined.[66] The context-specific function of NF-Y depends on its interaction with different cofactors.[59,60] We found that NFYa interacts with SP2 in the heart. It will be interesting to determine whether faulty regulation of their interaction affects heart development and contributes to congenital heart disease.

Metabolic state of fetal CMs

During early embryogenesis, the heart primarily uses anaerobic glycolysis for energy. Yet, by mid-to-late gestation, mammalian hearts transition to also utilize aerobic metabolism.[67,68] By the end of gestation, over 50% of ATP in newborn hearts comes from OXPHOS.[69] Defects in OXPHOS can cause serious heart defects and neonatal death,[70-77] as seen in *NFYa* cKO mice. The fetal heart primarily uses glucose as an energy source,[49,78] suggesting OXPHOS metabolism at this stage stems from glucose oxidation. Indeed, isotope tracing revealed that during mid-gestation, glucose fuels the TCA cycle in embryonic tissues, including the heart.[79] Glucose oxidation offers cellular growth benefits by producing precursors for biomass and yielding ATP through mitochondrial respiration. Furthermore, glucose oxidation, producing less ROS than fatty acid oxidation, supports CM proliferation.[37] This is evident when increasing glucose oxidation promoted CM proliferation, as seen in experiments with cardiac-specific deletion of *Pdk4*.[80] These observations suggest that glucose oxidation provides a metabolic state conducive to CM proliferation.

Our previous study showed neonatal regenerative CM4 cells have high expression of genes regulating both glycolysis and OXPHOS,[7] indicating a high level of glucose oxidation. However, the regulation of this metabolic state was unclear. Here, we identified NFYa as a

direct regulator of this metabolic state, as *NFYa* deletion caused embryonic lethality with metabolic defects and reduction of CM4 cells.

Different developmental states of fetal CMs

Through a multiomics approach, we identified several fetal CM subpopulations that shared the transcriptome signature of the neonatal regenerative CM4 cells. Although the precise lineage relationship between these fetal populations and the neonatal CM4 cells requires further investigation, our study showed that fetal CM4 cells in *NFYa* cKO hearts had decreased proliferation and cell count. Our previous study demonstrated a similar decline in the number of neonatal CM4 cells from P1 to P8,[7] coinciding with reduced *NFYa* expression. These results suggest that NFYa regulates the CM4 cell state. The decline of CM4 cells postnatally and in *NFYa* cKO hearts is potentially due to a cell state transition in response to loss of NFYa expression. Future orthogonal analyses, such as lineage tracing, are necessary to fully address this question. The varying maturity in fetal CM populations, possibly due to developmental origins or microenvironment, is unclear. Nevertheless, our study details their transcriptomic differences, aiding future research into these questions.

Limitations of the study

By integrating multiomics data, we aim to accurately identify fetal CM subpopulations. However, sequencing-based approaches might introduce artifacts in identifying cell clusters. Future experiments are required to validate these populations. Although the metabolic defect is most prominent in *NFYa* cKO hearts, it has not been directly tested if this is the cause of embryonic death. Rescuing experiments will definitively demonstrate that.

STAR★METHODS

RESOURCE AVAILABILITY

Lead contact—Further information and requests for resources and reagents should be directed to and will be fulfilled by the lead contact, Eric N. Olson (eric.olson@utsouthwestern.edu).

Material availability—New reagents generated from this study are available from the lead contact upon request.

Data and code availability—All data, including sequencing reads and single-nucleus expression matrices, have been deposited in NCBI's Gene Expression Omnibus (http://www.ncbi.nlm.nih.gov/geo/). The accession number for the snRNA-seq and snATATC data reported in this study is GEO: GSE232961. The accession number for the Visium spatial transcriptome data reported in this study is GEO: GSE232962. The accession number for ChIP-seq data reported in this study is GSE232960. All datasets generated in this study can be accessed under a GEO superseries with accession number GEO: GSE232963. Any additional information required to reanalyze the data reported in this paper is available from the lead contact upon request.

EXPERIMENTAL MODEL AND STUDY PARTICIPANT DETAILS

Experimental animals—All animal work described in this manuscript has been approved and conducted under the oversight of the UT Southwestern Institutional Animal Care and Use Committee (IACUC) as well as under the Boston Children's Hospital IACUC regulations. Timed-pregnant C57BL/6 mice *NFYa* cKO dams were used for embryonic analyses. Neonatal Sprague-Dawley rats (Envigo) were used to isolate neonatal rat ventricular cardiomyocytes (NRVMs). Animals were housed in a 12 h light/dark cycle in a temperature-controlled room in the Animal Research Center of UT Southwestern and AAALAC-accredited animal facilities at Boston Children's Hospital and monitored by full time staff, with ad libitum access to water and food. Sex was not determined for embryos and neonatal pups.

Cell lines—All cells were cultured at 37°C with 5% CO_2. Primary cardiomyocytes were isolated from P1-2 mice or rats using the Neomyt isolation kit from Cellutron Life Technologies (NC-6031). Isolated cardiomyocytes were maintained in Dulbecco's modified Eagle's medium (DMEM) (Sigma, D5796)/199 medium (Gibco, 11150-059) (3:1) with 3% fetal bovine serum (FBS) (Gemini Bio Products, 100-106), and 1% penicillin-streptomycin (Sigma, P0781). HEK 293 cells (Clontech, 632271) were maintained in DMEM with 10% FBS, and 1% penicillin-streptomycin.

METHOD DETAILS

Histology and immunochemistry—Animals were euthanized by isoflurane anesthesia followed by cervical dislocation and removal of hearts. Embryonic and postnatal mouse hearts were dissected and fixed in 4% paraformaldehyde (Electron Microscopy Sciences, 15710) in PBS (Sigma, D8537) at 4°C overnight, cryopreserved in 10% sucrose/PBS and 18% sucrose/PBS solution sequentially, embedded in O.C.T. Compound (Fisher Healthcare, 23730571), and cryosectioned at 10-μm intervals. Sections were stained for H&E (Abcam, ab245880) for morphological analysis and Picro Sirius Red (Abcam, ab15068) for analysis of fibrotic tissue.

For immunofluorescence staining, cryosections were washed with PBS twice and air-dried for 20 min at room temperature and fixed with 4%PFA for 10 min. Section slides were then washed twice with PBS and permeabilized with 0.3% Triton X-100 (Fisher Scientific, BP151-500) in PBS (PBST) for 10 min. Sections were then incubated in blocking solution (10% goat serum/3% BSA/0.025% Triton X-100/PBS) for 1 h and stained with the indicated primary antibodies diluted in blocking solution at 4°C overnight using the following dilutions: cTnT (Abcam, ab8295, 1:500), pH3 (Cell Signaling Technology,9701S, 1:250), NFYa (Abcam, ab154554, 1:250), Aurora B kinase (Abcam, ab2254, 1:200). Samples were subsequently washed with PBS three times (5 min for each wash) and incubated with corresponding secondary antibodies conjugated to Alexa Fluor 488, 555 or 647 (Invitrogen) prepared in blocking solution with Hoechst (Thermo Scientific, 62249, 1:1,000) at room temperature for 2 h. After secondary antibody incubation, samples were washed three times with PBS, then mounted with Prolong Diamond Antifade Mountant (Thermo Fisher Scientific, P36962). Images were obtained using a Zeiss LSM 800 confocal microscope and analyzed in ImageJ software. Antigen retrieval by epitope retrieval solution (IHC World) in

a steamer (IHC-Tek Epitope Retrieval Streamer Set) were used before permeabilization step for staining Aurora B kinase.

Joint single-nucleus RNA and ATAC profiling—Hearts at E15.5 were dissected and flash-frozen in liquid nitrogen. Genotyping was performed to ensure proper pooling of hearts with the same genotype. Four hearts were pooled for each sample. Cardiac nuclei were isolated using PCM1 antibody (Sigma-Aldrich, HPA023374) and cell sorting, as previously described.[7] Total cardiac nuclei were used to generate joint snRNA and snATAC libraries using Single Cell Multiome ATAC + Gene Expression (10×Genomics) according to the manufacturer's protocol. Sequencing was performed on an Illumina Nextseq 500 system operated by the Next Generation Sequencing Core of Children's Research Institute at UT Southwestern using the 150bp high output sequencing kit (Illumina).

The Cell Ranger Single-Cell Software Suite (https://support.10xgenomics.com/single-cell-geneexpression/software/pipelines/latest/what-is-cell-ranger) was used to perform sample demultiplexing, barcode processing, and single-cell 3′ gene counting. The cDNA reads were aligned to the mm10/GRCm38 pre-mRNA reference genome. We sequenced 4765 and 3974 CM nuclei from WT and *NFYa* KO hearts, respectively. We obtained average 2,531 genes and a median 103,550 peaks per cell. Outputs from the 10x Cellranger-ARC software package were processed using the Seurat[88] and Signac[81] packages. Briefly, cellranger-ARC aggr was run for combined WT and *NFYa* KO samples and generated a single feature-barcode matrix containing all the data that were normalized between samples. "Gene Expression" and "Peaks" files from cellranger-ARC output were used to construct Seurat objects in R. A shared peak set derived from the integration of peaks identified for each sample was used to analyze the snATAC dataset. The combined Seurat object was QC'd using the same metrics: 100 < nCount_ATAC < 100,000; 1000 < nCount_RNA< 100,000; and percent mitochondrial reads < 20. Next, doublets were identified and removed using Doubletfinder[89] on the RNA assay. Pre-processing and dimensional reduction were performed on the RNA and ATAC assays separately, using standard approaches for RNA and ATAC-seq data.[90] Gene expression UMI count data was normalized using SCTransform. LSI was used to perform dimension reduction on the DNA accessibility assay dataset on the LSI components 2:20. A WNN graph was generated using the weighted combination of the RNA and ATAC modalities. All downstream analysis were performed using features of Seurat/signac or using Seurat wrappers for other packages. Differential gene expression analyses were performed comparing clusters using the FindMarkers function on either the RNA assay, with thresholds of $| \log_2 FC | > 0.5$ and P-adj <0.05. Differential gene expression analysis was performed using the Wilcoxon test.

To identify putative regulators of each CM population, we searched for TFs whose expression is enriched in CM populations in the RNA measurements, but *also* have enriched accessibility for their motifs in the ATAC measurements. To do so, we ran two tests: one using gene expression data, and the other using chromVAR motif accessibilities. We calculated a p-value based on the Wilcox rank sum test, and we restricted our search to TFs that returned significant results in both tests.

To calculate CM4 gene expression score in individual CM nucleus, we took a list of CM4 marker genes (Figure 2G) and used the "AddModuleScore" function in Seurat on the SCT transformed RNA assay, which calculated averaged expression of all CM4 markers for each nucleus.

Spatial transcriptome analysis—Spatial transcriptome analysis on heart sections was performed using the Visium Spatial Gene Expression Reagents Kits (10×Genomics) according to the manufacturer's protocol and as described before.[91] Briefly, mouse hearts were dissected and immediately embedded in a tissue embedding mold filled with OCT and placed in a bath of isopentane and liquid nitrogen. OCT-embedded heart tissue blocks were cryosectioned in a cryostat to generate appropriately sized sections for Visium Spatial slides. 10 μm sections at the four-chamber view of WT and *NFYa* cKO hearts at E15.5 were collected and placed on the Visum Spatial slides capture areas. Sequencing was performed on an Illumina Nextseq 500 system operated by the Next Generation Sequencing Core of Children's Research Institute at UT Southwestern.

For data analysis, the Space Ranger Single-Cell Software Suite (https://support.10xgenomics.com/spatial-gene-expression/software/pipelines/latest/what-is-space-ranger) was used to perform sample demultiplexing, reads alignment, and to generate feature-spot matrices, as described in detail.[91] The cDNA reads were aligned to the mm10/GRCm38 mRNA reference genome. H&E staining images were supplemented to Spatial Ranger for tissue detection, fiducial detection, and alignment of the spatial position of sequenced data points. Further analyses were performed using the Seurat R package v4.2,[88] following the instruction (https://satijalab.Org/seurat/v3.2/spatial_vignette.html). To map the spatial location of the CM population from embryonic hearts that we identified from WT and *NFYa* cKO mice using Multiome (Figure 2B), we deconvoluted the spatial transcriptome by integrating it with the gene expression matrix from the multiome data using the TransferData function in Seurat. This analysis generated probability scores for each cell type at each capture spot, which correlate with cellular fraction and were used to generate pie-charts to show cellular composition. The spatial locations of each cell type were visualized using SpatialFeaturePlot in Seurat.

Measurement of *in vivo* oxygen consumption rates (OCR)—Primary CMs were isolated from *NFYa* $^{fl/fl}$ mice at P1 as described.[92] Isolated CMs were seeded in an Agilent Seahorse XFe96 Cell Culture Microplate (Agilent, 101085; FluxPak: Agilent, 102601-100) at a density of 50,000 cells per well. One day after seeding, control adenovirus (Ad-LacZ) or Cre adenovirus (Ad-Cre) were added to the cells. Agilent Mito Stress Test was performed using an Agilent Seahorse XFe96 Analyzer at 48h post infection following manufacturer's instructions. Oligomycin (Sigma–Aldrich, 75351-5MG) was loaded into port A at a final concentration of 1.5 μM. Carbonyl cyanide 4-(trifluoromethoxy) phenylhydrazone (FCCP; Sigma–Aldrich, C2920-10MG) was loaded into port B at a final concentration of 1.5 μM. Rotenone (Sigma–Aldrich, R8875-1G) and antimycin (Sigma–Aldrich, A8674-25MG) were loaded into port C at final concentrations of 0.5 μM. The running program consisted of 13 measurement cycles, including 4 cycles for baseline, and 3 cycles after treatment with each

drug. Each cycle included 2 min mix, 1 min wait and 2 min measure. Oxygen consumption rate (OCR) values were determined using the Seahorse software, Wave 2.4.0.

Measurement of reactive oxygen species (ROS)—To measure ROS levels in *NFYa* cKO CMs, we first isolated primary CMs from *NFYa* $^{fl/fl}$ mice at P1, as described previously.[92] One day after seeding, control adenovirus (Ad-LacZ) or Cre adenovirus (Ad-Cre) were added to the cells. Two days after infection, cells were incubated with CM-H2DCFDA (Invitrogen) at 5 μM for 1h at 37 °C in the dark. Cells were then recovered in growth medium for 2h followed by fluorescence recording and image acquisition. Fluorescence signals at excitation/emission 495/527 were recorded by a microplate reader. Fluorescent images were taken using an Olympus FV3000R resonant scanning confocal microscope.

Metabolomics—Whole heart tissues from *E15* control (*αMHC-Cre;NFYa*$^{fl/+}$ or *αMHC-Cre;NFYa*$^{+/+}$) and *NFYa* cKO mice were harvested. To avoid possible contamination by metabolites present in the blood, dissected hearts were bathed in cold PBS, followed by tender massage, triggering them to expel any remaining blood. This process was carried out for both *NFYa cKO* and control hearts to maintain consistency in our experimental approach. Heart samples were then flash-frozen in liquid nitrogen. Frozen samples were next homogenized in bead tubes with Precellys Evolution (3× 20 s at 6800 rpm) in 1 ml of methanol/water (80:20 vol/vol). 200 μl of sample were transferred to a new tube with 800 μl of ice-cold methanol/water (80:20 vol/vol). Samples were vortexed for 1 min and centrifuged at 20,000 × g for 15 min at 4 °C. Supernatant was transferred to a new tube and dried with SpeedVac system. Samples were further processed for targeted metabolomics analysis as described.[93] Briefly, samples were reconstituted in 0.03% formic acid, vortexed, and debris was removed by centrifugation. The supernatant was used for the metabolomic studies. Prior to MS acquisition, samples were normalized to residual protein in the supernatant, to prevent contamination of the instrument. Next, liquid chromatography with tandem mass spectrometry (LC-MS/MS) was performed with AB QTRAP 5500 liquid chromatography–triple quadrupole mass spectrometer (Applied Biosystems SCIEX). Two mobile phases were used for separation: 0.03% formic acid in water and 0.03% formic acid in acetonitrile (ACN). MultiQuant software v.2.1 (Applied Biosystems SCIEX) was used to review the chromatogram and integrate peak area. The peak area for each metabolite was normalized to the total ion count (TIC). TIC normalization was performed to account for any ionization inefficiencies between samples, as previously performed.[94,95] The acquired data was searched against an in-house database comprised of approximately 580 metabolites. This database was curated using a kit of 600 standards purchased from Sigma in well-plate format and from other individual standards purchased over time. Each standard has been confirmed by accurate mass, retention time, and MS2 fragmentation. and to give equal loading of sample material onto the column and into the mass spec. From our samples, 368 metabolites were detected above the baseline set by cell-free samples. Differentially enriched pathways were determined by Fisher’s exact test in R statistical package. Differentially regulated metabolites were determined using cutoffs of p value of <0.05.

Electron transport chain activity measurements—Embryonic hearts were snap frozen in liquid nitrogen. Total heart tissue was then homogenized in 10 mM MOPS, 1 mM EDTA, pH 7.4 and mitochondria lysed upon sonication. As a measure of the combined activities of complexes I, III, and IV, NADH oxidation sensitive to inhibition by rotenone (complex I inhibitor) was measured spectrophotometrically as the rate of NADH consumption (340 nm, ε = 6,200 M-1 cm-1) using total heart lysates in a buffer containing 10 mM MOPS and 10 mM KCl at pH = 7.4, as previously described.[37] NADH (100 μM) was added to initiate electron transport and activity was normalized to total protein in the assay.

ChIP-seq—ChIP-seq was carried out as previously described,[96,97] with modifications. Adenovirus expressing TY1 tagged NFYa was used to infect NRVMs for 48h. Two 15cm plates yielding 5-10 million cells were used for each ChIP sample. Cells were detached from the plate with trypsin and fixed in 1% PFA in PBS at room temperature for 8 min then quenched with 0.125 M glycine for 10 min. Crosslinked samples were then washed with cold PBS and resuspended in Farnham Lab buffer (5mM PIPEs PH8, 85 mM KCcl, 0.5% NP40) for sonication based nuclear extraction. Specifically, resuspended cells were sonicated on a Bioruptor Pico (Diagenode) for 6 cycles (10 sec on/30 sec off for each cycle) at 4°C. Successful nuclear extraction was verified using Trypan Blue. After nuclear extraction, nuclei were collected by centrifugation and resuspended in sonication buffer (0.1% SDS, 1% Triton X-100, 10mM Tris-HCl, 1 mM EDTA, 0.1% sodium deoxycholate, 0.25% sarkosyl, 1 mM DTT, 1x cOmplete Protease Inhibitor Cocktail (Roche), and 200 μM PMSF, pH 8.0). Chromatin sonication was performed on a Bioruptor Pico (Diagenode) for 20 cycles (30 sec on/30 sec off for each cycle) 4°C. After sonication, 1% of the sonicated chromatin from each sample was taken out as 'Input' samples. The remaining sonicated chromatin was evenly split for NFYa-TY1 or H3k27ac ChIP. NaCl was then added to a final concentration of 300 mM for histone ChIP and 150 mM for transcription factor ChIP. 1 μg/mL H3k27ac antibody (Diagenode, C15410196) or 4 μg/mL Ty1 tag antibody (Diagenode, C152000054) was added to each sample and incubated at 4°C overnight with gentle rotation. The next day, 30 μL/mL of pre-washed Dynabeads Protein G (Invitrogen, 10004D) was added to each sample for a two-hour incubation. After that, the beads were washed and eluted for DNA as done before.[96] ChIP-seq libraries were prepared using the NEBNext Ultra II DNA Library Preparation Kit complemented with NEBNext Multiplex Oligos for Illumina from NEB.

ChIP-seq analysis was performed as described before.[97] Raw reads were processed with Samtools (Verson 0.1.18)[82] and aligned to rat (Rn6) genome assembly using Bowtie2 (Version 2.3.4)[83] with default parameters. MACS2 (Version 2.1.1)[84] was applied to each sample to perform peaking calling using the "-nomodel" parameter with the input sample. For motif analysis, chromatin peaks of NFYa ChIP were searched for known motifs in the JASPAR database using HOMER (Version 4.8)[85] "analyzing genomic positions" function with "-size = 500". ChIP-seq tracks were plotted using Deeptools.[86]

Quantitative real-time PCR analysis—Total RNA was extracted from heart tissues using Trizol and reverse transcribed using iScript Reverse Transcription

Supermix (Bio-Rad) with random primers. The Quantitative Polymerase Chain Reactions (qPCR) were assembled using KAPA SYBR Fast qPCR Master Mix (KAPA, KK4605). Assays were performed using a 7900HT Fast Real-Time PCR machine (Applied Biosystems). Expression values were normalized to 18S mRNA and were represented as fold change. The following oligonucleotides were ordered from Integrated DNA Technologies to measure transcript abundance: 18S Forward: 5′- ACC GCA GCT AGG AAT AAT GGA - 3′; 18S Reverse: 5′- GCC TCA GTT CCG AAA ACC A - 3′; NFYa Forward: 5′- GGTGGACAAGGCCAAACCATC- 3′; NFYa Reverse: 5′- TCTGCTGGGTTTGACCCTGC- 3′; MtND1 Forward: 5′- CTAGCAGAAACAAACCGGGC - 3′; MtND1 Reverse: 5′- CCGGCTGCGTATTCTACGTT - 3′; 16S Forward: 5′- CCGCAAGGGAAAGATGAAAGAC - 3′; 16S Reverse: 5′- TCGTTTGGTTTCGGGGTTTC-3′.

Reporter assay—The multiplex reporter assay was performed as described before,[98,99] with modifications. The GFP-tag sequence from the 13 DNA-tag vectors reporter system[98] was individually cloned into a modified pGL4.23 vector (Promega) that already contained a mammalian minimal SCP1 promoter.[100] The NFYa-bound promoter regions of *Pgk1, Atp5b, Cox8a* based on ChIP-seq were PCR-amplified and cloned into the multiple cloning sites upstream of the SCP1 promoter. An empty vector without an additional DNA insert was used as the negative control. Plasmids were transfected into HEK293 cells, in which plasmids with different tags were mixed at equal molar ratios. The negative control vector was co-transfected in each batch. Cells were collected 48 h after transfection. DNA and RNA were extracted using the AllPrep DNA/RNA Micro Kit (Qiagen) following the manufacturer's protocol. QPCR experiments were performed on both DNA and cDNA templates using primers specific to each tag-DNA.[98] To calculate the enhancer activity, the relative expression level of each tag compared to the negative control (result from cDNA) was normalized to the amount of transfected DNA.[98]

Proximity biotinylation and protein identification by mass spectrometry—The study utilized proximity biotinylation (BioID) as previously described.[101] Two independent BioID experiments were conducted. NRVM cells were isolated, cultured and infected with adenovirus expressing NFYa-miniTurbo. Eight confluent 15 cm dishes of NRVMs were used for each replicate. Four of these dishes were treated with 50 μM biotin in NRVMs culture media for 2 hours (BIO+). The remaining four dishes were used as negative controls and were left untreated (BIO−). Cell lysates were extracted in 1 ml of lysis buffer (RIPA lysis buffer, 6 M urea, supplemented with cOmplete protease inhibitor cocktail and PhosSTOP phosphatase inhibitor cocktail) and mechanically lysed with a 27-gauge syringe. Lysates were added to 9 ml of dilution buffer (50 mM Tris, 150 mM NaCl) and 100μl of equilibrated streptavidin magnetic beads (88816, ThermoFisher). Lysates were incubated overnight at 4°C. Beads were washed 5 times with lysis buffer and boiled for 5 min in 2x Laemmli sample buffer (1610737, Bio-Rad). After boiling, samples were run for 1 cm in an Any-KD Mini-PROTEAN 10-well gel (4569034, Bio-Rad). Gels were then fixed and stained with EZBlue (G1041, Sigma). The area of the gel containing proteins was cut into small 1 mm

cubes and submitted for analysis to the Proteomics Core Facility at the University of Texas Southwestern Medical Center.

For proteomics analysis, gel bands containing protein samples were digested overnight with trypsin (Pierce) following reduction and alkylation with DTT and iodoacetamide (Sigma). The samples then underwent solid phase extraction cleanup with an Oasis HLB plate (Waters) and the resulting samples were injected onto an Orbitrap Fusion Lumos mass spectrometer coupled to an Ultimate 3000 RSLC-Nano liquid chromatography system. Raw MS data files were analyzed using Proteome Discoverer v2.2 (ThermoFisher), with peptide identification performed using Sequest HT searching against the rat protein database from UniProt. Fragment and precursor tolerances of 14 10 ppm and 0.6 Da were specified, and three missed cleavages were allowed. The false-discovery rate (FDR) cutoff was 1% for all peptides. Protein abundance values were calculated by normalizing the protein abundances obtained from cells pulsed with biotin (BIO+) to the abundance of the same protein purified in un- pulsed cells (BIO−). Protein hits were obtained by filtering results from both experiments (>20-fold enrichment in “Biotin” samples to “Control” samples) and were used for analysis on GO.

Protein immunoprecipitation assays—Immunoprecipitations were performed as previously described in detail.[102,103] $NFYA^{Flag}$ was co-expressed with $LacZ^{Myc}$ or $SP2^{Myc}$ in HEK293 cells for 48h. Pre-cleared cell lysates were incubated with Flag magnetic beads (Sigma, M8823) overnight. The Flag epitope tag was eluted using 0.5 mg ml^{-1} free 3× Flag peptide (Sigma). The final elution and input obtained before immunoprecipitation were analyzed by western blot using an anti-Myc (Invitrogen) or rabbit anti-Flag antibody (Sigma). For immunoprecipitation from neonatal CMs, CMs from P2 mouse hearts were isolated and cultured as described above. Roughly 200ug of protein lysate was incubated with 8ug of NFYa antibody (Abcam, ab6558) or IgG (Diagenode, C15410206) at 4°C overnight, then with 100ul of Dynabeads protein G (Invitrogen) for 4 hours, followed by washes as described before.[102,103] Western blots were performed using the final elution from the beads with anti-NFYa (Santa Cruz, cs-17753) or anti-SP2 (Abcam, ab229468) antibodies.

Wholemount tissue imaging—*NFYa* cKO hearts were dissected and fixed in 4%PFA at 4°C overnight. Tissue was cleared using the EZ clear method.[104] Cleared hearts were stained with 1 μg/mL Propidium Iodide Solution in PBS at room temperature overnight. Images were acquired using a Leica SP8 confocal microscope. Images were rendered in 3D and analyzed using Bitplane Imaris v7.7.1.

Gene ontology analysis—Gene ontology analysis of differentially expressed genes from indicated comparisons was performed using Metascape.[87] Gene ontology analysis of indicated ChIP-Seq peaks was performed using Genomic Regions Enrichment of Annotations Tool (GREAT, Version 3.0.0) with “Basal plus extension” setting.[105]

QUANTIFICATION AND STATISTICAL ANALYSIS

Statistical analyses were performed using GraphPad Prism 8 (GraphPad Software Inc) using statistical tests mentioned in each analysis, with p-value < 0.05 considered significant unless otherwise indicated. All data are displayed as mean ± SEM unless otherwise indicated.

Supplementary Material

Refer to Web version on PubMed Central for supplementary material.

ACKNOWLEDGMENTS

We thank Drs. Jian Xu and Yoon Jung Kim from the Children's Research Institute at the University of Texas Southwestern Medical Center (UTSW) for Illumina sequencing, Dr. Yichi Zhang and the Metabolomics Core (UTSW) for targeted metabolomic analysis, the Proteomics Core (UTSW) for BioID proteomics analysis, and Dr. Sankar Maity (MD Anderson) for providing $NFYa^{fl/fl}$ mice. M.C. is supported by a K99/R00 grant (NHLBI, K99HL153683, and R00HL1536833). This work was supported by grants from the NIH (HL-130253, HL-157281, and HD-087351), the Foundation Leducq Transatlantic Networks of Excellence in Cardiovascular Research, and the Robert A. Welch Foundation (grant 1-0025).

INCLUSION AND DIVERSITY

We support inclusive, diverse, and equitable conduct of research.

REFERENCES

1. Alkass K, Panula J, Westman M, Wu TD, Guerquin-Kern JL, and Bergmann O (2015). No evidence for cardiomyocyte number expansion in preadolescent mice. Cell 163, 1026–1036. 10.1016/j.cell.2015.10.035. [PubMed: 26544945]
2. Guo Y, and Pu WT (2020). Cardiomyocyte maturation: new phase in development. Circ. Res 126, 1086–1106. 10.1161/CIRCRESAHA.119.315862. [PubMed: 32271675]
3. Gan P, Wang Z, Morales MG, Zhang Y, Bassel-Duby R, Liu N, and Olson EN (2022). RBPMS is an RNA-binding protein that mediates cardiomyocyte binucleation and cardiovascular development. Dev. Cell 57, 959–973.e7. 10.1016/j.devcel.2022.03.017. [PubMed: 35472321]
4. Tomita-Mitchell A, Stamm KD, Mahnke DK, Kim MS, Hidestrand PM, Liang HL, Goetsch MA, Hidestrand M, Simpson P, Pelech AN, et al. (2016). Impact of MYH6 variants in hypoplastic left heart syndrome. Physiol. Genomics 48, 912–921. 10.1152/physiol-genomics.00091.2016. [PubMed: 27789736]
5. Porrello ER, Johnson BA, Aurora AB, Simpson E, Nam YJ, Matkovich SJ, Dorn GW 2nd, van Rooij E, and Olson EN (2011). MiR-15 family regulates postnatal mitotic arrest of cardiomyocytes. Circ. Res 109, 670–679. 10.1161/CIRCRESAHA.111.248880. [PubMed: 21778430]
6. Porrello ER, Mahmoud AI, Simpson E, Johnson BA, Grinsfelder D, Canseco D, Mammen PP, Rothermel BA, Olson EN, and Sadek HA (2013). Regulation of neonatal and adult mammalian heart regeneration by the miR-15 family. Proc. Natl. Acad. Sci. USA 110, 187–192. 10.1073/pnas.1208863110. [PubMed: 23248315]
7. Cui M, Wang Z, Chen K, Shah AM, Tan W, Duan L, Sanchez-Ortiz E, Li H, Xu L, Liu N, et al. (2020). Dynamic transcriptional responses to injury of regenerative and non-regenerative cardiomyocytes revealed by single-nucleus RNA sequencing. Dev. Cell 53, 102–116.e8. 10.1016/j.devcel.2020.02.019. [PubMed: 32220304]
8. Porrello ER, Mahmoud AI, Simpson E, Hill JA, Richardson JA, Olson EN, and Sadek HA (2011). Transient regenerative potential of the neonatal mouse heart. Science 331, 1078–1080. 10.1126/science.1200708. [PubMed: 21350179]
9. Ye L, D'Agostino G, Loo SJ, Wang CX, Su LP, Tan SH, Tee GZ, Pua CJ, Pena EM, Cheng RB, et al. (2018). Early regenerative capacity in the porcine heart. Circulation 138, 2798–2808. 10.1161/CIRCULATIONAHA.117.031542. [PubMed: 30030417]

10. Zhu W, Zhang E, Zhao M, Chong Z, Fan C, Tang Y, Hunter JD, Borovjagin AV, Walcott GP, Chen JY, et al. (2018). Regenerative potential of neonatal porcine hearts. Circulation 138, 2809–2816. 10.1161/CIRCULATIONAHA.118.034886. [PubMed: 30030418]
11. Haubner BJ, Schneider J, Schweigmann U, Schuetz T, Dichtl W, Velik-Salchner C, Stein JI, and Penninger JM (2016). Functional recovery of a human neonatal heart after severe myocardial infarction. Circ. Res 118, 216–221. 10.1161/CIRCRESAHA.115.307017. [PubMed: 26659640]
12. Yoshida H, Okada T, Haze K, Yanagi H, Yura T, Negishi M, and Mori K (2001). Endoplasmic reticulum stress-induced formation of transcription factor complex ERSF including NF-Y (CBF) and activating transcription factors 6alpha and 6beta that activates the mammalian unfolded protein response. Mol. Cell. Biol 21, 1239–1248. 10.1128/MCB.21.4.1239-1248.2001. [PubMed: 11158310]
13. Xiong S, Chirala SS, and Wakil SJ (2000). Sterol regulation of human fatty acid synthase promoter I requires nuclear factor-Y- and Sp-1-binding sites. Proc. Natl. Acad. Sci. USA 97, 3948–3953. 10.1073/pnas.040574197. [PubMed: 10759542]
14. Dooley KA, Millinder S, and Osborne TF (1998). Sterol regulation of 3-hydroxy-3-methylglutaryl-coenzyme A synthase gene through a direct interaction between sterol regulatory element binding protein and the trimeric CCAAT-binding factor/nuclear factor Y. J. Biol. Chem 273, 1349–1356. 10.1074/jbc.273.3.1349. [PubMed: 9430668]
15. Yamanaka T, Miyazaki H, Oyama F, Kurosawa M, Washizu C, Doi H, and Nukina N (2008). Mutant huntingtin reduces HSP70 expression through the sequestration of NF-Y transcription factor. EMBO J. 27, 827–839. 10.1038/emboj.2008.23. [PubMed: 18288205]
16. Di Agostino S, Strano S, Emiliozzi V, Zerbini V, Mottolese M, Sacchi A, Blandino G, and Piaggio G (2006). Gain of function of mutant p53: the mutant p53/NF-Y protein complex reveals an aberrant transcriptional mechanism of cell cycle regulation. Cancer Cell 10, 191–202. 10.1016/j.ccr.2006.08.013. [PubMed: 16959611]
17. Bhattacharya A, Deng JM, Zhang Z, Behringer R, de Crombrugghe B, and Maity SN (2003). The B subunit of the CCAAT box binding transcription factor complex (CBF/NF-Y) is essential for early mouse development and cell proliferation. Cancer Res. 63, 8167–8172. [PubMed: 14678971]
18. Basile V, Baruffaldi F, Dolfini D, Belluti S, Benatti P, Ricci L, Artusi V, Tagliafico E, Mantovani R, Molinari S, et al. (2016). NF-YA splice variants have different roles on muscle differentiation. Biochim. Biophys. Acta 1859, 627–638. 10.1016/j.bbagrm.2016.02.011. [PubMed: 26921500]
19. Farina A, Manni I, Fontemaggi G, Tiainen M, Cenciarelli C, Bellorini M, Mantovani R, Sacchi A, and Piaggio G (1999). Down-regulation of cyclin B1 gene transcription in terminally differentiated skeletal muscle cells is associated with loss of functional CCAAT-binding NF-Y complex. Oncogene 18, 2818–2827. 10.1038/sj.onc.1202472. [PubMed: 10362252]
20. Gurtner A, Manni I, Fuschi P, Mantovani R, Guadagni F, Sacchi A, and Piaggio G (2003). Requirement for down-regulation of the CCAAT-binding activity of the NF-Y transcription factor during skeletal muscle differentiation. Mol. Biol. Cell 14, 2706–2715. 10.1091/mbc.e02-09-0600. [PubMed: 12857858]
21. Lindahl GE, Chambers RC, Papakrivopoulou J, Dawson SJ, Jacobsen MC, Bishop JE, and Laurent GJ (2002). Activation of fibroblast procollagen alpha 1(I) transcription by mechanical strain is transforming growth factor-beta-dependent and involves increased binding of CCAAT-binding factor (CBF/NF-Y) at the proximal promoter. J. Biol. Chem 277, 6153–6161. 10.1074/jbc.M108966200. [PubMed: 11748224]
22. Chen J (2021). NF-Y is critical for the proper growth of zebrafish embryonic heart and its cardiomyocyte proliferation. Genesis 59, e23408. 10.1002/dvg.23408. [PubMed: 33417743]
23. Agah R, Frenkel PA, French BA, Michael LH, Overbeek PA, and Schneider MD (1997). Gene recombination in postmitotic cells. Targeted expression of Cre recombinase provokes cardiac-restricted, site-specific rearrangement in adult ventricular muscle in vivo. J. Clin. Invest 100, 169–179. 10.1172/JCI119509. [PubMed: 9202069]
24. Kodo K, Ong SG, Jahanbani F, Termglinchan V, Hirono K, InanlooRahatloo K, Ebert AD, Shukla P, Abilez OJ, Churko JM, et al. (2016). iPSC-derived cardiomyocytes reveal abnormal TGF-β signalling in left ventricular non-compaction cardiomyopathy. Nat. Cell Biol 18, 1031–1042. 10.1038/ncb3411. [PubMed: 27642787]

25. Luxán G, Casanova JC, Martínez-Poveda B, Prados B, D'Amato G, MacGrogan D, Gonzalez-Rajal A, Dobarro D, Torroja C, Martinez F, et al. (2013). Mutations in the NOTCH pathway regulator MIB1 cause left ventricular noncompaction cardiomyopathy. Nat. Med 19, 193–201. 10.1038/nm.3046. [PubMed: 23314057]

26. Kim JY, Jeong HS, Chung T, Kim M, Lee JH, Jung WH, and Koo JS (2017). The value of phosphohistone H3 as a proliferation marker for evaluating invasive breast cancers: A comparative study with Ki67. Oncotarget 8, 65064–65076. 10.18632/onco-target.17775. [PubMed: 29029412]

27. Hao Y, Hao S, Andersen-Nissen E, Mauck WM 3rd, Zheng S, Butler A, Lee MJ, Wilk AJ, Darby C, Zager M, et al. (2021). Integrated analysis of multimodal single-cell data. Cell 184, 3573–3587.e29. 10.1016/j.cell.2021.04.048. [PubMed: 34062119]

28. Ames EG, Lawson MJ, Mackey AJ, and Holmes JW (2013). Sequencing of mRNA identifies re-expression of fetal splice variants in cardiac hypertrophy. J. Mol. Cell. Cardiol 62, 99–107. 10.1016/j.yjmcc.2013.05.004. [PubMed: 23688780]

29. Cui M, Wang Z, Bassel-Duby R, and Olson EN (2018). Genetic and epigenetic regulation of cardiomyocytes in development, regeneration and disease. Development 145, dev171983. 10.1242/dev.171983. [PubMed: 30573475]

30. Taegtmeyer H, Sen S, and Vela D (2010). Return to the fetal gene program: a suggested metabolic link to gene expression in the heart. Ann. N. Y. Acad. Sci 1188, 191–198. 10.1111/j.1749-6632.2009.05100.x. [PubMed: 20201903]

31. Wu M. (2018). Mechanisms of trabecular formation and specification during cardiogenesis. Pediatr. Cardiol 39, 1082–1089. 10.1007/s00246-018-1868-x. [PubMed: 29594501]

32. Medioni C, Bertrand N, Mesbah K, Hudry B, Dupays L, Wolstein O, Washkowitz AJ, Papaioannou VE, Mohun TJ, Harvey RP, et al. (2010). Expression of Slit and Robo genes in the developing mouse heart. Dev. Dyn 239, 3303–3311. 10.1002/dvdy.22449. [PubMed: 20941780]

33. Li Y, Tian X, Zhao H, He L, Zhang S, Huang X, Zhang H, Miquerol L, and Zhou B (2018). Genetic targeting of Purkinje fibres by Sema3a-CreERT2. Sci. Rep 8, 2382. 10.1038/s41598-018-20829-9. [PubMed: 29403069]

34. Gan P, Patterson M, Velasquez A, Wang K, Tian D, Windle JJ, Tao G, Judge DP, Makita T, Park TJ, et al. (2019). Tnni3k alleles influence ventricular mononuclear diploid cardiomyocyte frequency. PLoS Genet. 15, e1008354. 10.1371/journal.pgen.1008354. [PubMed: 31589606]

35. Patterson M, Barske L, Van Handel B, Rau CD, Gan P, Sharma A, Parikh S, Denholtz M, Huang Y, Yamaguchi Y, et al. (2017). Frequency of mononuclear diploid cardiomyocytes underlies natural variation in heart regeneration. Nat. Genet 49, 1346–1353. 10.1038/ng.3929. [PubMed: 28783163]

36. Nakada Y, Nhi Nguyen NU, Xiao F, Savla JJ, Lam NT, Abdisalaam S, Bhattacharya S, Mukherjee S, Asaithamby A, Gillette TG, et al. (2019). DNA damage response mediates pressure overload-induced cardiomyocyte hypertrophy. Circulation 139, 1237–1239. 10.1161/CIRCULATIONAHA.118.034822. [PubMed: 30802166]

37. Puente BN, Kimura W, Muralidhar SA, Moon J, Amatruda JF, Phelps KL, Grinsfelder D, Rothermel BA, Chen R, Garcia JA, et al. (2014). The oxygen-rich postnatal environment induces cardiomyocyte cell-cycle arrest through DNA damage response. Cell 157, 565–579. 10.1016/j.cell.2014.03.032. [PubMed: 24766806]

38. Mahmoud AI, Kocabas F, Muralidhar SA, Kimura W, Koura AS, Thet S, Porrello ER, and Sadek HA (2013). Meis1 regulates postnatal cardiomyocyte cell cycle arrest. Nature 497, 249–253. 10.1038/nature12054. [PubMed: 23594737]

39. DeLaughter DM, Bick AG, Wakimoto H, McKean D, Gorham JM, Kathiriya IS, Hinson JT, Homsy J, Gray J, Pu W, et al. (2016). Single-cell resolution of temporal gene expression during heart development. Dev. Cell 39, 480–90. 10.1016/j.devcel.2016.10.001. [PubMed: 27840107]

40. Veugelers M, De Cat B, Ceulemans H, Bruystens AM, Coomans C, Dürr J, Vermeesch J, Marynen P, and David G (1999). Glypican-6, a new member of the glypican family of cell surface heparan sulfate proteoglycans. J. Biol. Chem 274, 26968–26977. 10.1074/jbc.274.38.26968. [PubMed: 10480909]

41. Ng SY, Wong CK, and Tsang SY (2010). Differential gene expressions in atrial and ventricular myocytes: insights into the road of applying embryonic stem cell-derived cardiomyocytes for

future therapies. Am. J. Physiol. Cell Physiol 299, C1234–C1249. 10.1152/ajp-cell.00402.2009. [PubMed: 20844252]

42. van Ouwerkerk AF, Bosada FM, van Duijvenboden K, Houweling AC, Scholman KT, Wakker V, Allaart CP, Uhm JS, Mathijssen IB, Baartscheer T, et al. (2022). Patient-specific TBX5-G125R variant induces profound transcriptional deregulation and atrial dysfunction. Circulation 145, 606–619. 10.1161/CIRCULATIONAHA.121.054347. [PubMed: 35113653]
43. Bruneau BG, Nemer G, Schmitt JP, Charron F, Robitaille L, Caron S, Conner DA, Gessler M, Nemer M, Seidman CE, et al. (2001). A murine model of Holt-Oram syndrome defines roles of the T-box transcription factor Tbx5 in cardiogenesis and disease. Cell 106, 709–721. 10.1016/S0092-8674(01)00493-7. [PubMed: 11572777]
44. Sweat ME, Cao Y, Zhang X, Burnicka-Turek O, Perez-Cervantes C, Akerberg BN, Ma Q, Wakimoto H, Gorham JM, Song MK, et al. (2023). Tbx5 maintains atrial identity by regulating an atrial enhancer network. Preprint at bioRxiv. 10.1101/2023.04.21.537535.
45. Chen Y, Xiao D, Zhang L, Cai CL, Li BY, and Liu Y (2021). The role of Tbx20 in cardiovascular development and function. Front. Cell Dev. Biol 9, 638542. 10.3389/fcell.2021.638542. [PubMed: 33585493]
46. Goodyer WR, Beyersdorf BM, Paik DT, Tian L, Li G, Buikema JW, Chirikian O, Choi S, Venkatraman S, Adams EL, et al. (2019). Transcriptomic profiling of the developing cardiac conduction system at single-cell resolution. Circ. Res 125, 379–397. 10.1161/CIRCRESAHA.118.314578. [PubMed: 31284824]
47. Nadadur RD, Broman MT, Boukens B, Mazurek SR, Yang X, van den Boogaard M, Bekeny J, Gadek M, Ward T, Zhang M, et al. (2016). Pitx2 modulates a Tbx5-dependent gene regulatory network to maintain atrial rhythm. Sci. Transl. Med 8, 354ra115. 10.1126/scitranslmed.aaf4891.
48. Wang J, Klysik E, Sood S, Johnson RL, Wehrens XH, and Martin JF (2010). Pitx2 prevents susceptibility to atrial arrhythmias by inhibiting left-sided pacemaker specification. Proc. Natl. Acad. Sci. USA 107, 9753–9758. 10.1073/pnas.0912585107. [PubMed: 20457925]
49. Piquereau J, and Ventura-Clapier R (2018). Maturation of cardiac energy metabolism during perinatal development. Front. Physiol 9, 959. 10.3389/fphys.2018.00959. [PubMed: 30072919]
50. Werner JC, Whitman V, Musselman J, and Schuler HG (1982). Perinatal changes in mitochondrial respiration of the rabbit heart. Biol. Neonate 42, 208–216. 10.1159/000241601. [PubMed: 6891604]
51. Zhao Q, Sun Q, Zhou L, Liu K, and Jiao K (2019). Complex regulation of mitochondrial function during cardiac development. J. Am. Heart Assoc 8, e012731. 10.1161/JAHA.119.012731. [PubMed: 31215339]
52. Acin-Perez R, Benador IY, Petcherski A, Veliova M, Benavides GA, Lagarrigue S, Caudal A, Vergnes L, Murphy AN, Karamanlidis G, et al. (2020). A novel approach to measure mitochondrial respiration in frozen biological samples. EMBO J. 39, e104073. 10.15252/embj.2019104073. [PubMed: 32432379]
53. Wu G, Fang YZ, Yang S, Lupton JR, and Turner ND (2004). Glutathione metabolism and its implications for health. J. Nutr 134, 489–92. 10.1093/jn/134.3.489. [PubMed: 14988435]
54. Hovi T, Allison AC, Raivio K, and Vaheri A (1977). Purine metabolism and control of cell proliferation. Ciba Found. Symp 48, 225–248. 10.1002/9780470720301.ch14.
55. Mills RJ, Titmarsh DM, Koenig X, Parker BL, Ryall JG, Quaife-Ryan GA, Voges HK, Hodson MP, Ferguson C, Drowley L, et al. (2017). Functional screening in human cardiac organoids reveals a metabolic mechanism for cardiomyocyte cell cycle arrest. Proc. Natl. Acad. Sci. USA 114, E8372–E8381. 10.1073/pnas.1707316114. [PubMed: 28916735]
56. Peng Y, and Jahroudi N (2002). The NFY transcription factor functions as a repressor and activator of the von Willebrand factor promoter. Blood 99, 2408–2417. 10.1182/blood.v99.7.2408. [PubMed: 11895773]
57. Li Y, Xiao X, Chen H, Chen Z, Hu K, and Yin D (2020). Transcription factor NFYA promotes G1/S cell cycle transition and cell proliferation by transactivating cyclin D1 and CDK4 in clear cell renal cell carcinoma. Am. J. Cancer Res 10, 2446–2463. [PubMed: 32905496]
58. Oldfield AJ, Henriques T, Kumar D, Burkholder AB, Cinghu S, Paulet D, Bennett BD, Yang P, Scruggs BS, Lavender CA, et al. (2019). NF-Y controls fidelity of transcription initiation at

gene promoters through maintenance of the nucleosome-depleted region. Nat. Commun 10, 3072. 10.1038/s41467-019-10905-7. [PubMed: 31296853]

59. Maity SN (2017). NF-Y (CBF) regulation in specific cell types and mouse models. Biochim. Biophys. Acta Gene Regul. Mech 1860, 598–603. 10.1016/j.bbagrm.2016.10.014. [PubMed: 27815195]
60. Fleming JD, Pavesi G, Benatti P, Imbriano C, Mantovani R, and Struhl K (2013). NF-Y coassociates with FOS at promoters, enhancers, repetitive elements, and inactive chromatin regions, and is stereo-positioned with growth-controlling transcription factors. Genome Res. 23, 1195–1209. 10.1101/gr.148080.112. [PubMed: 23595228]
61. Branon TC, Bosch JA, Sanchez AD, Udeshi ND, Svinkina T, Carr SA, Feldman JL, Perrimon N, and Ting AY (2018). Efficient proximity labeling in living cells and organisms with TurboID. Nat. Biotechnol 36, 880–887. 10.1038/nbt.4201. [PubMed: 30125270]
62. Monroe TO, Hill MC, Morikawa Y, Leach JP, Heallen T, Cao S, Krijger PHL, de Laat W, Wehrens XHT, Rodney GG, et al. (2019). YAP partially reprograms chromatin accessibility to directly induce adult cardiogenesis in vivo. Dev. Cell 48, 765–779.e7. 10.1016/j.devcel.2019.01.017. [PubMed: 30773489]
63. Xin M, Kim Y, Sutherland LB, Murakami M, Qi X, McAnally J, Porrello ER, Mahmoud AI, Tan W, Shelton JM, et al. (2013). Hippo pathway effector Yap promotes cardiac regeneration. Proc. Natl. Acad. Sci. USA 110, 13839–13844. 10.1073/pnas.1313192110. [PubMed: 23918388]
64. Reed BD, Charos AE, Szekely AM, Weissman SM, and Snyder M (2008). Genome-wide occupancy of SREBP1 and its partners NFY and SP1 reveals novel functional roles and combinatorial regulation of distinct classes of genes. PLoS Genet. 4, e1000133. 10.1371/journal.pgen.1000133. [PubMed: 18654640]
65. Benatti P, Chiaramonte ML, Lorenzo M, Hartley JA, Hochhauser D, Gnesutta N, Mantovani R, Imbriano C, and Dolfini D (2016). NF-Y activates genes of metabolic pathways altered in cancer cells. Oncotarget 7, 1633–1650. 10.18632/oncotarget.6453. [PubMed: 26646448]
66. Poluri RTK, Paquette V, Allain ÉP, Lafront C, Joly-Beauparlant C, Weidmann C, Droit A, Guillemette C, Pelletier M, and Audet-Walsh É (2021). KLF5 and NFYA factors as novel regulators of prostate cancer cell metabolism. Endocr. Relat. Cancer 28, 257–271. 10.1530/ERC-20-0504. [PubMed: 33690159]
67. Gaspar JA, Doss MX, Hengstler JG, Cadenas C, Hescheler J, and Sachinidis A (2014). Unique metabolic features of stem cells, cardiomyocytes, and their progenitors. Circ. Res 114, 1346–1360. 10.1161/CIRCRESAHA.113.302021. [PubMed: 24723659]
68. Lopaschuk GD, and Jaswal JS (2010). Energy metabolic phenotype of the cardiomyocyte during development, differentiation, and postnatal maturation. J. Cardiovasc. Pharmacol 56, 130–140. 10.1097/FJC.0b013e3181e74a14. [PubMed: 20505524]
69. Spielmann H, and Lücke I (1973). Changes in the respiratory activity of different tissues of rat and mouse embryos during development. Naunyn Schmiedebergs Arch. Pharmacol 278, 151–164. 10.1007/BF00500647. [PubMed: 4268640]
70. Baker CN, Gidus SA, Price GF, Peoples JN, and Ebert SN (2015). Impaired cardiac energy metabolism in embryos lacking adrenergic stimulation. Am. J. Physiol. Endocrinol. Metab 308, E402–E413. 10.1152/ajpendo.00267.2014. [PubMed: 25516547]
71. Dorn GW 2nd, Vega RB, and Kelly DP (2015). Mitochondrial biogenesis and dynamics in the developing and diseased heart. Genes Dev. 29, 1981–1991. 10.1101/gad.269894.115. [PubMed: 26443844]
72. Ingraham CA, Burwell LS, Skalska J, Brookes PS, Howell RL, Sheu SS, and Pinkert CA (2009). NDUFS4: creation of a mouse model mimicking a Complex I disorder. Mitochondrion 9, 204–210. 10.1016/j.mito.2009.02.001. [PubMed: 19460290]
73. Larsson NG, Wang J, Wilhelmsson H, Oldfors A, Rustin P, Lewandoski M, Barsh GS, and Clayton DA (1998). Mitochondrial transcription factor A is necessary for mtDNA maintenance and embryogenesis in mice. Nat. Genet 18, 231–236. 10.1038/ng0398-231. [PubMed: 9500544]
74. Menendez-Montes I, Escobar B, Palacios B, Gómez MJ, Izquierdo-Garcia JL, Flores L, Jiménez-Borreguero LJ, Aragones J, Ruiz-Cabello J, Torres M, et al. (2016). Myocardial VHL-HIF

signaling controls an embryonic metabolic switch essential for cardiac maturation. Dev. Cell 39, 724–739. 10.1016/j.devcel.2016.11.012. [PubMed: 27997827]

75. Mohammed S, Bahitham W, Chan A, Chiu B, Bamforth F, and Sergi C (2012). Mitochondrial DNA related cardiomyopathies. Front. Biosci. (Elite Ed.) 4, 1706–1716. [PubMed: 22201986]
76. Schiff M, Ogier de Baulny H, and Lombès A (2011). Neonatal cardiomyopathies and metabolic crises due to oxidative phosphorylation defects. Semin. Fetal Neonatal Med 16, 216–221. 10.1016/j.siny.2011.04.002. [PubMed: 21606011]
77. Zhang D, Li Y, Heims-Waldron D, Bezzerides V, Guatimosim S, Guo Y, Gu F, Zhou P, Lin Z, Ma Q, et al. (2018). Mitochondrial cardiomyopathy caused by elevated reactive oxygen species and impaired cardiomyocyte proliferation. Circ. Res 122, 74–87. 10.1161/CIRCRESAHA.117.311349. [PubMed: 29021295]
78. Onay-Besikci A. (2006). Regulation of cardiac energy metabolism in newborn. Mol. Cell. Biochem 287, 1–11. 10.1007/s11010-006-9123-9. [PubMed: 16670818]
79. Solmonson A, Faubert B, Gu W, Rao A, Cowdin MA, Menendez-Montes I, Kelekar S, Rogers TJ, Pan C, Guevara G, et al. (2022). Compartmentalized metabolism supports midgestation mammalian development. Nature 604, 349–353. 10.1038/s41586-022-04557-9. [PubMed: 35388219]
80. Cardoso AC, Lam NT, Savla JJ, Nakada Y, Pereira AHM, Elnwasany A, Menendez-Montes I, Ensley EL, Petric UB, Sharma G, et al. (2020). Mitochondrial substrate utilization regulates cardiomyocyte cell cycle progression. Nat. Metab 2, 167–178. [PubMed: 32617517]
81. Stuart T, Srivastava A, Madad S, Lareau CA, and Satija R (2021). Single-cell chromatin state analysis with Signac. Nat. Methods 18, 1333–1341. 10.1038/s41592-021-01282-5. [PubMed: 34725479]
82. Li H, Handsaker B, Wysoker A, Fennell T, Ruan J, Homer N, Marth G, Abecasis G, and Durbin R; 1000 Genome Project Data Processing Subgroup (2009). The Sequence Alignment/Map format and SAMtools. Bioinformatics 25, 2078–2079. 10.1093/bioinformatics/btp352. [PubMed: 19505943]
83. Langmead B, and Salzberg SL (2012). Fast gapped-read alignment with Bowtie 2. Nat. Methods 9, 357–359. 10.1038/nmeth.1923. [PubMed: 22388286]
84. Zhang Y, Liu T, Meyer CA, Eeckhoute J, Johnson DS, Bernstein BE, Nusbaum C, Myers RM, Brown M, Li W, et al. (2008). Model-based analysis of ChIP-Seq (MACS). Genome Biol. 9, R137. 10.1186/gb-2008-9-9-r137. [PubMed: 18798982]
85. Heinz S, Benner C, Spann N, Bertolino E, Lin YC, Laslo P, Cheng JX, Murre C, Singh H, and Glass CK (2010). Simple combinations of lineage-determining transcription factors prime cis-regulatory elements required for macrophage and B cell identities. Mol. Cell 38, 576–589. 10.1016/j.molcel.2010.05.004. [PubMed: 20513432]
86. Ramírez F, Ryan DP, Grüning B, Bhardwaj V, Kilpert F, Richter AS, Heyne S, Dündar F, and Manke T (2016). deepTools2: a next generation web server for deep-sequencing data analysis. Nucleic Acids Res. 44, W160–W165. 10.1093/nar/gkw257. [PubMed: 27079975]
87. Zhou Y, Zhou B, Pache L, Chang M, Khodabakhshi AH, Tanaseichuk O, Benner C, and Chanda SK (2019). Metascape provides a biologist-oriented resource for the analysis of systems-level datasets. Nat. Commun 10, 1523. 10.1038/s41467-019-09234-6. [PubMed: 30944313]
88. Butler A, Hoffman P, Smibert P, Papalexi E, and Satija R (2018). Integrating single-cell transcriptomic data across different conditions, technologies, and species. Nat. Biotechnol 36, 411–420. 10.1038/nbt.4096. [PubMed: 29608179]
89. McGinnis CS, Murrow LM, and Gartner ZJ (2019). DoubletFinder: doublet detection in single-cell RNA sequencing data using artificial nearest neighbors. Cell Syst. 8, 329–337.e4. 10.1016/j.cels.2019.03.003. [PubMed: 30954475]
90. Hafemeister C, and Satija R (2019). Normalization and variance stabilization of single-cell RNA-seq data using regularized negative binomial regression. Genome Biol. 20, 296. 10.1186/s13059-019-1874-1. [PubMed: 31870423]
91. Cui M, Atmanli A, Morales MG, Tan W, Chen K, Xiao X, Xu L, Liu N, Bassel-Duby R, and Olson EN (2021). Nrf1 promotes heart regeneration and repair by regulating proteostasis and redox balance. Nat. Commun 12, 5270. 10.1038/s41467-021-25653-w. [PubMed: 34489413]

92. Yücel D, Garay BI, Perlingeiro RCR, and van Berlo JH (2022). Stimulation of cardiomyocyte proliferation is dependent on species and level of maturation. Front. Cell Dev. Biol 10, 806564. 10.3389/fcell.2022.806564. [PubMed: 35663393]

93. Mullen AR, Hu Z, Shi X, Jiang L, Boroughs LK, Kovacs Z, Boriack R, Rakheja D, Sullivan LB, Linehan WM, et al. (2014). Oxidation of alpha-ketoglutarate is required for reductive carboxylation in cancer cells with mitochondrial defects. Cell Rep. 7, 1679–1690. 10.1016/j.celrep.2014.04.037. [PubMed: 24857658]

94. Pachnis P, Wu Z, Faubert B, Tasdogan A, Gu W, Shelton S, Solmonson A, Rao AD, Kaushik AK, Rogers TJ, et al. (2022). In vivo isotope tracing reveals a requirement for the electron transport chain in glucose and glutamine metabolism by tumors. Sci. Adv 8, eabn9550. 10.1126/sciadv.abn9550. [PubMed: 36044570]

95. Tasdogan A, Faubert B, Ramesh V, Ubellacker JM, Shen B, Solmonson A, Murphy MM, Gu Z, Gu W, Martin M, et al. (2020). Metabolic heterogeneity confers differences in melanoma metastatic potential. Nature 577, 115–120. 10.1038/s41586-019-1847-2. [PubMed: 31853067]

96. Shah AM, Guo L, Morales MG, Jaichander P, Chen K, Huang H, Cano Hernandez K, Xu L, Bassel-Duby R, Olson EN, et al. (2023). TWIST2-mediated chromatin remodeling promotes fusion-negative rhabdomyosarcoma. Sci. Adv 9, eade8184. 10.1126/sciadv.ade8184. [PubMed: 37115930]

97. Wang Z, Cui M, Shah AM, Ye W, Tan W, Min YL, Botten GA, Shelton JM, Liu N, Bassel-Duby R, et al. (2019). Mechanistic basis of neonatal heart regeneration revealed by transcriptome and histone modification profiling. Proc. Natl. Acad. Sci. USA 116, 18455–18465. 10.1073/pnas.1905824116. [PubMed: 31451669]

98. Nam J, Dong P, Tarpine R, Istrail S, and Davidson EH (2010). Functional cis-regulatory genomics for systems biology. Proc. Natl. Acad. Sci. USA 107, 3930–3935. 10.1073/pnas.1000147107. [PubMed: 20142491]

99. He D, Wu D, Muller S, Wang L, Saha P, Ahanger SH, Liu SJ, Cui M, Hong SJ, Jain M, et al. (2021). miRNA-independent function of long noncoding pri-miRNA loci. Proc. Natl. Acad. Sci. USA 118. e2017562118. 10.1073/pnas.2017562118. [PubMed: 33758101]

100. Juven-Gershon T, Cheng S, and Kadonaga JT (2006). Rational design of a super core promoter that enhances gene expression. Nat. Methods 3, 917–922. 10.1038/nmeth937. [PubMed: 17124735]

101. Cannavino J, Shao M, An YA, Bezprozvannaya S, Chen S, Kim J, Xu L, McAnally JR, Scherer PE, Liu N, et al. (2021). Regulation of cold-induced thermogenesis by the RNA binding protein FAM195A. Proc. Natl. Acad. Sci. USA 118. e2104650118. 10.1073/pnas.2104650118. [PubMed: 34088848]

102. Anderson DM, Anderson KM, Chang CL, Makarewich CA, Nelson BR, McAnally JR, Kasaragod P, Shelton JM, Liou J, Bassel-Duby R, et al. (2015). A micropeptide encoded by a putative long noncoding RNA regulates muscle performance. Cell 160, 595–606. 10.1016/j.cell.2015.01.009. [PubMed: 25640239]

103. Makarewich CA, Baskin KK, Munir AZ, Bezprozvannaya S, Sharma G, Khemtong C, Shah AM, McAnally JR, Malloy CR, Szweda LI, et al. (2018). MOXI is a mitochondrial micropeptide that enhances fatty acid β-oxidation. Cell Rep. 23, 3701–3709. 10.1016/j.celrep.2018.05.058. [PubMed: 29949755]

104. Hsu CW, Cerda J 3rd, Kirk JM, Turner WD, Rasmussen TL, Flores Suarez CP, Dickinson ME, and Wythe JD (2022). EZ clear for simple, rapid, and robust mouse whole organ clearing. eLife 11, e77419. 10.7554/eLife.77419. [PubMed: 36218247]

105. McLean CY, Bristor D, Hiller M, Clarke SL, Schaar BT, Lowe CB, Wenger AM, and Bejerano G (2010). GREAT improves functional interpretation of cis-regulatory regions. Nat. Biotechnol 28, 495–501. 10.1038/nbt.1630. [PubMed: 20436461]

Highlights

- Deleting *NFYa* in cardiomyocytes results in cardiac noncompaction and embryonic death
- Fetal cardiomyocyte subtypes identified by multi-modal single-cell transcriptomics
- *NFYa* deletion alters cardiomyocyte composition and mitochondrial metabolism
- NFYa, working with SP2, activates metabolic gene transcription

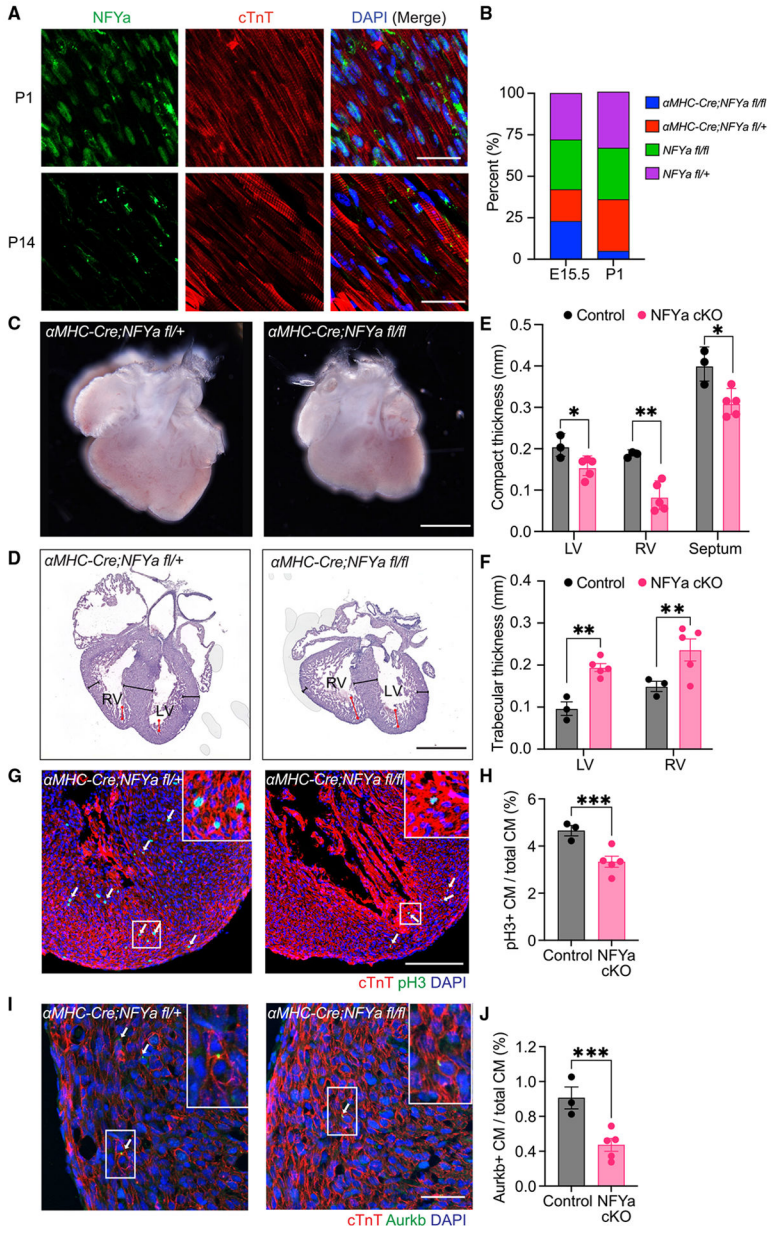

Figure 1. Cardiomyocyte-specific deletion of *NFYa* causes embryonic lethality

(A) Immunofluorescent staining of NFYa and cardiac troponin T (cTnT) on P1 and P14 hearts. Scale bars, 25 μm.

(B) Percentage of genotypes observed at E15.5 and P1. *NFYa* cKO (*αMHC-Cre;NFYa*$^{fl/fl}$) is shown in blue.

(C) Micrographs of representative control (*αMHC-Cre;NFYa*$^{fl/+}$) and *NFYa* cKO hearts at E15.5. Scale bars, 500 μm.

(D) Hematoxylin and eosin (H&E) staining images of representative control and *NFYa* cKO hearts at E15.5. Black lines mark the compact myocardium zone, and red lines mark the trabecular zone. LV, Left ventricle; RV, right ventricle. Scale bars, 500 μm.

(E) Thickness of the compact myocardium in the LV, RV, and septum.

(F) Thickness of the LV and RV trabecular regions.

(G) Immunofluorescence staining for pH3, cTnT, and DAPI of control and *NFYa* cKO hearts at E15.5. White arrows indicate $pH3^+$ CMs. Scale bars, 100 μm.

(H) Quantification of $pH3^+$ CMs over total CMs.

(I and J) Immunofluorescence staining for Aurkb, cTnT, and DAPI of control and *NFYa* cKO hearts at E15.5 (I) and quantification of $Aurkb^+$ midbody frequency (J). Scale bars, 25 μm. White arrows indicate $Aurkb^+$ midbodies between nuclei. All data are presented as mean ± SEM. *$p < 0.05$, **$p < 0.01$, ***$p < 0.001$ by Student's t test (E and F) and *z* test (H and J).

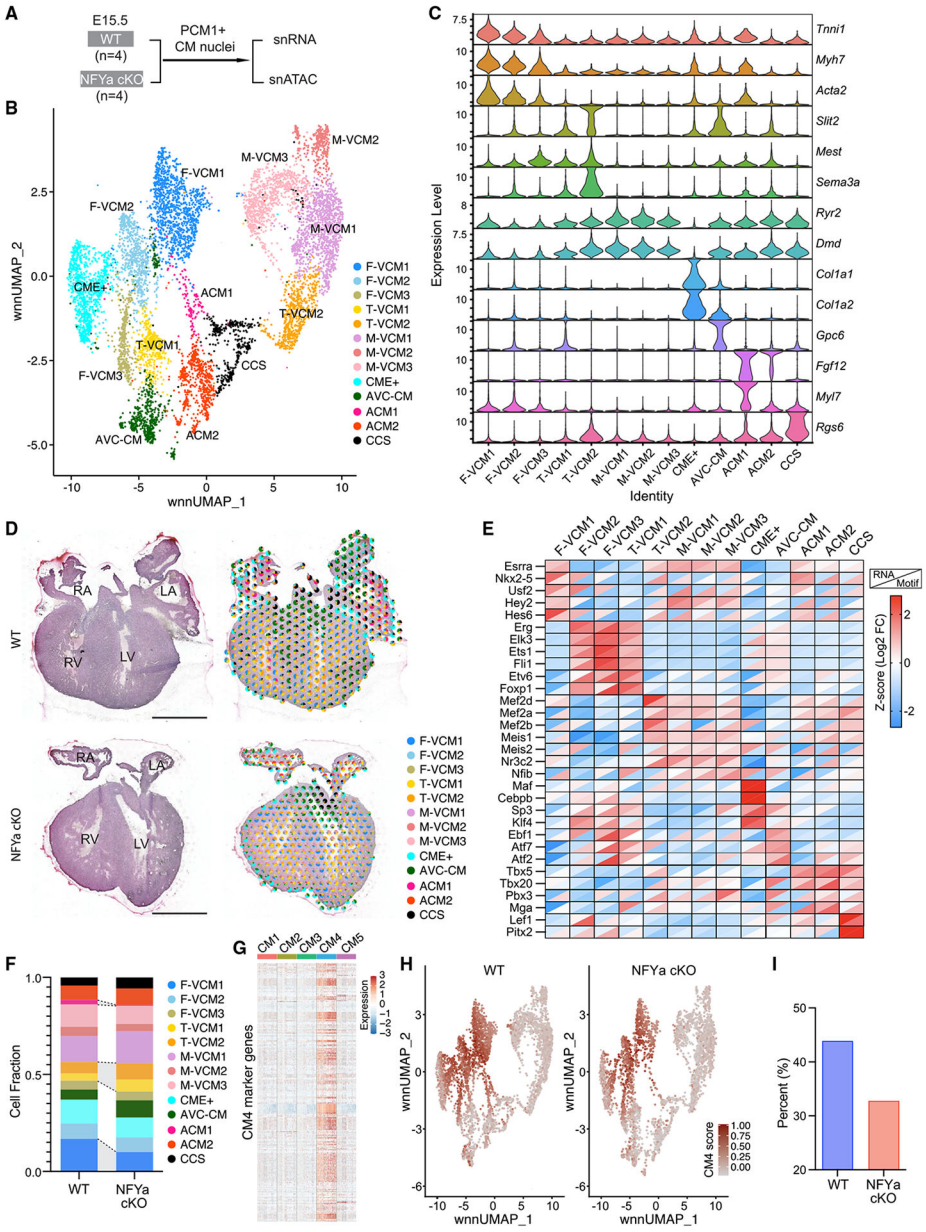

Figure 2. Change of cardiomyocyte composition upon *NFYa* deletion

(A) Schematics of joint single-nucleus RNA and ATAC sequencing from WT and *NFYa* cKO hearts at E15.5.

(B) UMAP shows CM populations from combined samples in (A).

(C) Violin plots showing the expression of representative marker genes for each CM population.

(D) Left, H&E images of WT and *NFYa* cKO hearts at E15.5. Right, cell type composition shown in pie charts for individual spatial spots sequenced from heart sections. Left and right ventricles (LV, RV) and atria (LA, RA) are indicated. Scale bars, 500 μm.

(E) Heatmap showing RNA expression enrichment (upper triangle) from snRNA-seq and corresponding motif accessibility (lower triangles) from scATAC-seq for representative transcriptional regulators of each identified CM population.
(F) Fraction of each CM population in WT and *NFYa* cKO hearts.
(G) Heatmap showing expression of CM4 marker genes in CM1-5 cells, identified from our previous study.[7]
(H) Averaged expression of CM4 marker genes (CM4 score) in each CM from WT and *NFYa* cKO hearts.
(I) Percentage of cells with high CM4 marker expression from WT and *NFYa* cKO hearts.

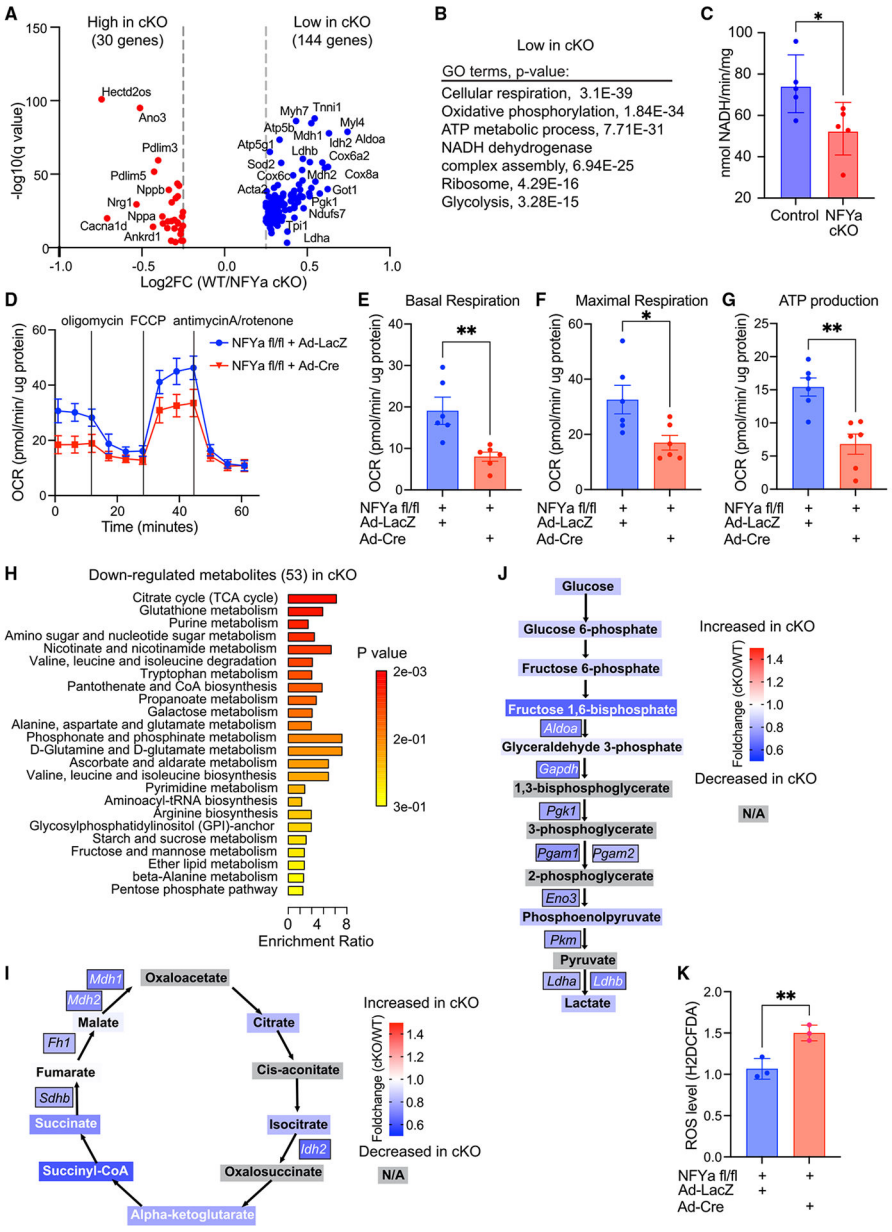

Figure 3. Metabolic dysregulation in *NFYa* cKO hearts

(A) Differentially expressed genes in *NFYa* cKO CMs compared with WT CMs. All CMs identified from the Multiome sequencing were analyzed.

(B) GO terms for downregulated genes in *NFYa* cKO CMs.

(C) NADH consumption by the electron transport chain at the mitochondrial membrane of *NFYa* cKO hearts and control hearts (*αMHC-Cre;NFYa*$^{fl/+}$ *or αMHC-Cre;NFYa*$^{+/+}$).

(D) Seahorse mitochondrial stress test showing oxygen consumption rates (OCRs) in neonatal *NFYa* $^{fl/fl}$ CMs infected with control (Ad-LacZ) or Cre (Ad-Cre) adenovirus. Drug addition is indicated.

(E–G) OCR measurements of basal respiration (E), maximal respiration (F), and ATP production (G) in control (Ad-LacZ) and *NFYa* KO (Ad-Cre) CMs from (D).

(H) Metabolic pathways downregulated in *NFYa* cKO hearts.
(I and J) Fold-change of metabolites in the TCA cycle (I) and glycolysis (J) along with gene expression changes for key enzymes regulating these metabolic pathways in snRNA-seq data. Box color depicts the fold-change (cKO/WT), and blue indicates decrease in cKO and red indicates increase in cKO. Metabolites marked in gray were not included in the analysis. Only genes with significant changes from snRNA-seq data are shown.
(K) Quantification of ROS levels in $NFYa^{fl/fl}$ CMs infected with Ad-LacZ or Ad-Cre. All data are presented as mean ± SEM. *$p < 0.05$, **$p < 0.01$ by Student's t test.

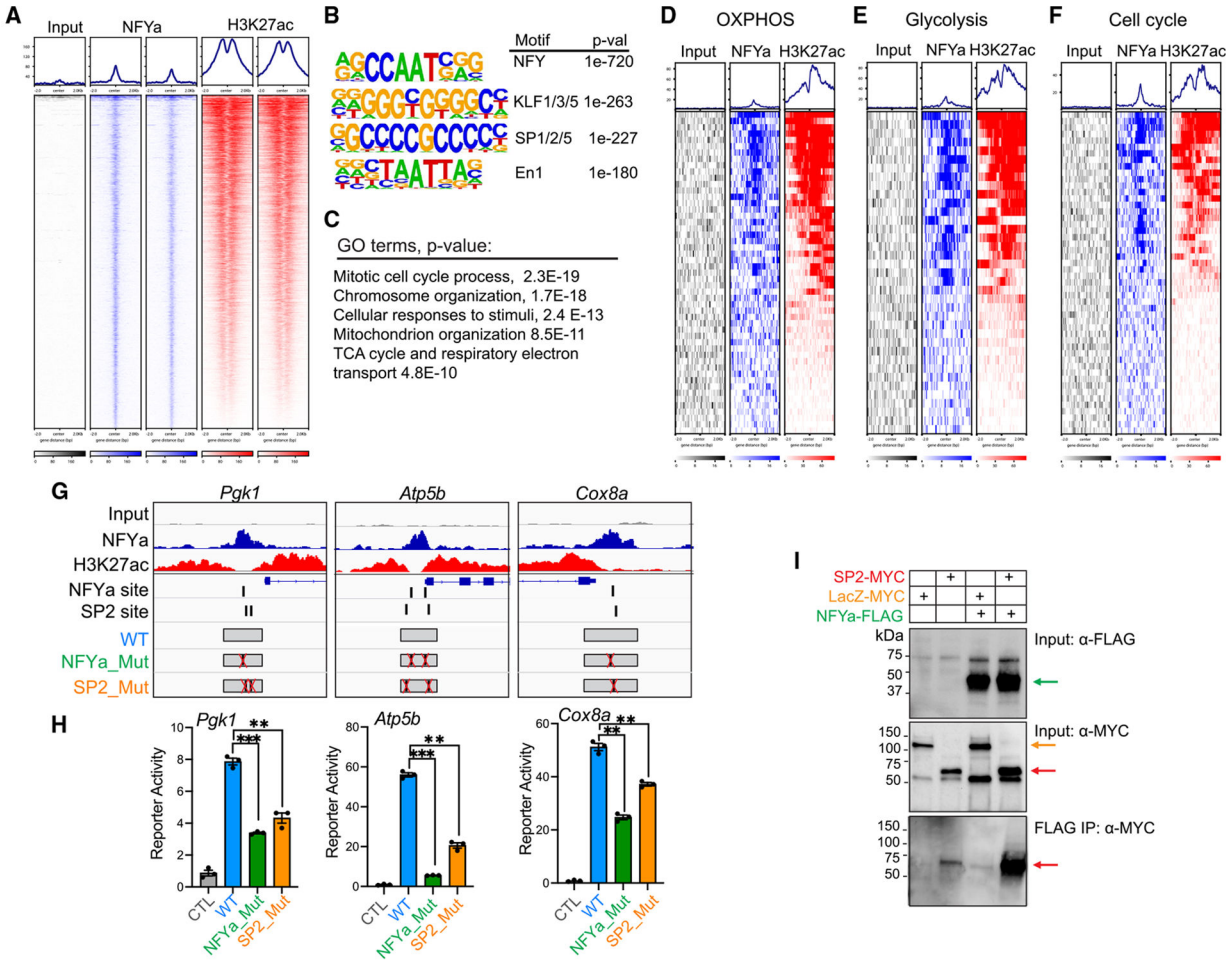

Figure 4. NFYa directly regulates the transcription of metabolic genes

(A) NFYa and H3K27ac ChIP-seq signals at NFYa-bound genomic regions in CMs.

(B) Top enriched motifs at NFYa-bound genomic regions.

(C) GO terms of the nearest genes associated with NFYa-bound regions.

(D–F) NFYa and H3K27ac ChIP-seq signals at promoter regions of genes regulating OXPHOS (D), glycolysis (E), and cell cycle (F).

(G) Schematics showing WT and mutant promoter regions of *Pgk1, Atp5b*, and *Cox8a* used for the reporter assay. NFYa and H3K27ac ChIP-seq signals are shown along with predicted NFYa and SP2 binding sites.

(H) Reporter activity driven by WT and mutant promoters normalized to minimal promoter control (CTL).

(I) Protein co-immunoprecipitation detects SP2 protein by NFYa pull-down. Green arrow marks NFYa-FLAG, yellow arrow marks LacZ-Myc, and red arrows mark SP2-Myc. All data are presented as mean ± SEM. **p < 0.01, ***p < 0.001, by Student's t test.

KEY RESOURCES TABLE

REAGENT or RESOURCE	SOURCE	IDENTIFIER
Antibodies		
Anti-PCM1 antibody produced in rabbit	Sigma-Aldrich	Cat#HPA023374; RRID:AB_1855073
Cardiac Troponin T Monoclonal Antibody (13-11)	Invitrogen	Cat#MA5-12960; RRID:AB_11000742
NFYa Antibody for IF and western	Santa Cruz	Cat#cs-17753 RRID:AB_628018
c-Myc monoclonal Antibody	Invitrogen	Cat# MA1-980
Monoclonal Anti-FLAG M2 antibody	Sigma	Cat#F3165 RRID:AB_259529
NFYa Antibody for IP	Abcam	Cat#ab6558 RRID:AB_305566
Rabbit IgG Antibody	Diagenode	Cat#C15410206 RRID:AB_2722554
Phospho-Histone H3 (Ser10) Antibody	Cell Signaling Technology	Cat#9701S; RRID:AB_331535
Aurora B Antibody	Abcam	Cat#Ab2254 RRID:AB_302923
SP2 Antibody	Abcam	Cat# ab229468
TY1 Antibody	Diagenode	Cat# C15200054
H3K27ac Antibody	Diagenode	Cat# C15410196 RRID:AB_2637079
Goat anti-Rabbit IgG (H+L) Cross-Adsorbed Secondary Antibody, Alexa Fluor 647	Invitrogen	Cat#A21244; RRID:AB_141663
Goat anti-Mouse IgG (H+L) Cross-Adsorbed Secondary Antibody, Alexa Fluor 488	Invitrogen	Cat#A-11001; RRID:AB_2534069
Goat anti-Mouse IgG (H+L) Cross-Adsorbed Secondary Antibody, Alexa Fluor 647	Invitrogen	Cat#A-21235; RRID:AB_2535804
Goat anti-Rabbit IgG (H+L) Cross-Adsorbed Secondary Antibody, Alexa Fluor 555	Invitrogen	Cat#A-21428; RRID:AB_2535849
Donkey anti-Goat IgG (H+L) Cross-Adsorbed Secondary Antibody, Alexa Fluor 555	Invitrogen	Cat#A-21432; RRID:AB_2535853
Bacterial and Virus Strains		
Stellar Competent Cells	Takara	Cat#636766
Adeno-Cre	This paper	N/A
Adeno-LacZ	This paper	N/A
Adeno-NFYa-miniTurbo	This paper	N/A
Chemicals, Peptides, and Recombinant Proteins		
Dulbecco's Modified Eagle's Medium - high glucose	Sigma-Aldrich	Cat#D5796
Medium 199, Earle's Salts	Gibco	Cat#11150-059
Fetal Bovine Serum	Gemini Bio Products	Cat#100-106
Penicillin-Streptomycin	Sigma-Aldrich	Cat#P0781
cOmplete Protease Inhibitor Cocktail	Roche	Cat#11697498001
RNaseOUT Recombinant Ribonuclease Inhibitor	Invitrogen	Cat#10777019
Hoechst 33342	Invitrogen	Cat#H3570
DAPI (4',6-Diamidino-2-Phenylindole, Dihydrochloride)	Invitrogen	Cat#D1306
Wheat Germ Agglutinin, Alexa Fluor™ 647 Conjugate	Invitrogen	Cat#W32466

L-Glutamine	Gibco	Cat#25030081
Glucose solution	Gibco	Cat#A2494001
Sodium pyruvate	Gibo	Cat#11360070
oligomycin A	Sigma	Cat#75351
FCCP	Sigma	Cat#C2920
Antimycin A	Sigma	Cat#A8674
Rotenone	Sigma	Cat#R8875
Propidium Iodide	ThermoFisher	Cat#P1304MP
Critical Commercial Assays		
Visium Spatial Gene Expression Slide & Reagent Kit	10xGenomics	Cat#PN- 1000187
Chromium Next GEM Single Cell Multiome ATAC + Gene Expression Reagent kit	10xGenomics	Cat# PN-1000285
Chromium Next GEM Chip J Single Cell Kit	10xGenomics	Cat# PN-1000234
Dual Index Kit TT Set A	10xGenomics	Cat# PN-1000215
D5000 High Sensitivity DNA ScreenTape	Agilent	Cat#5067-5592
D1000 ScreenTape	Agilent	Cat#5067-5582
Qubit dsDNA HS Assay Kit	Invitrogen	Cat#Q32854
Adeno-X Adenoviral System 3	Clontech	Cat#632267
RNeasy Mini Kit	Qiagen	Cat#74104
NEBNext Ultra II DNA Library Preparation Kit	NEB	Cat#E7103
iScript Reverse Transcription Supermix for RT-qPCR	Bio-Rad	Cat#1708840
KAPA SYBR Fast qPCR Master Mix	KAPA	Cat#KK4605
CM-H2DCFDA	Invitrogen	Cat#C6827
Seahorse XFe96 FluxPak mini	Agilent	Cat#102601-100
XF DMEM Medium	Agilent	Cat#103575-100
Deposited Data		
Raw and processed data	This paper	GEO: GSE232963
Experimental Models: Cell Lines		
Adeno-X 293 cells	Clontech	Cat#632271
Experimental Models: Organisms/Strains		
Mouse: C57BL/6J	The Jackson Laboratory	N/A
Mouse: NFYA $^{fl/fl}$, C57BL/6J	Dr. Sankar Maity (MD Anderson)	N/A
Mouse: aMHC-Cre, C57BL/6J	The Jackson Laboratory	Strain#:009074
Oligonucleotides		
Primer: 18S Forward: 5′- ACC GCA GCT AGG AAT AAT GGA - 3′	This paper	N/A
Primer: 18S Reverse: 5′- GCC TCA GTT CCG AAA ACC A - 3′	This paper	N/A
Primer: NFYa Forward: 5′- GGTGGACAAGGCCAAACCATC- 3′	This paper	N/A
Primer: NFYa Reverse: 5′- TCTGCTGGGTTTGACCCTGC- 3′	This paper	N/A
Primer: MtND1 Forward: 5′- CTAGCAGAAACAAACCGGGC - 3′	This paper	N/A

Primer: MtND1 Reverse: 5′- CCGGCTGCGTATTCTACGTT - 3′	This paper	N/A
Primer: 16S Forward: 5′- CCGCAAGGGAAAGATGAAAGAC - 3′	This paper	N/A
Primer: 16S Reverse: 5′-TCGTTTGGTTTCGGGGTTTC-3’	This paper	N/A
Recombinant DNA		
pGL4.23	Promega	Cat#9PIE841
pAdenoX-CMV	Takara	Cat#632269
Software and Algorithms		
Cell Ranger-ARC	10xGenomics	https://support.10xgenomics.com/single-cell-multiome-atac-gex/software/pipelines/latest/what-is-cell-ranger-arc
Seurat v4.0	Stuart et al.[81]	https://satijalab.org/seurat/
Signac v0.2.5	Stuart et al.[81]	https://stuartlab.org/signac/
FastQC v0.11.4	Babraham Bioinformatics	https://www.bioinformatics.babraham.ac.uk/projects/fastqc/
Samtools v0.1.18	Li et al.[82]	http://samtools.sourceforge.net/
Bowtie2 Version 2.3.4	Langmead et al., 2012[83]	https://bowtie-bio.sourceforge.net/bowtie2/index.shtml
MACS v2.1.1	Zhang et al. 2008[84]	https://pypi.org/project/MACS2/
Homer v4.8	Heinz et al. 2010[85]	http://homer.ucsd.edu/homer/introduction/install.html
Deeptools2	Ramírez et al., 2016[86]	https://deeptools.readthedocs.io/en/develop/
ImageJ	NIH	https://imagej.nih.gov/ij/index.html
Metascape	Zhou et al.[87]	http://metascape.org
GraphPad Prism 8	GraphPad Software Inc	N/A